Division of Solid Mechanics

ISRN LUTFD2/TFHF--06/5123--SE (1-83)

FE-MODELLING OF PC/ABS
- EXPERIMENTAL TESTS AND SIMULATIONS

Master's Dissertation by
Fredrik Nordgren and Maria Nyquist

Supervisors
Vijay Sharan, Sony Ericsson
Henrik Persson, Sony Ericsson
Mathias Wallin, Div. of Solid Mechanics
Paul Håkansson, Div. of Solid Mechanics

Printed by Media-Tryck, Lund, Sweden.

For information, address:
Division of Solid Mechanics, Lund University, Box 118, SE-221 00 Lund, Sweden.
Homepage: http://www.solid.lth.se

Preface

The Master's Thesis was preformed during the spring and summer of 2006 on the inquiry of Sony Ericsson Communication AB and supervision from the Division of Solid Mechanics, Lund University in Sweden.

There are many people who have helped and guided us throughout the project. We would like to thank those, whom without it would not have been possible to complete the project. Especially, we would like to express our gratitude to *Candidate for the doctorate* Paul Håkansson and *Dr.* Mathias Wallin, Solid Mechanics, for many valuable discussions and good advices.

Another special thank is to *Staff Engineer* Henrik Persson and his co-workers in the simulation and calculation group, Sony Ericsson, for valuable support and many enlightening advices.

Finally, we would like to thank *Senior Specialist* Tommy Sandevi, Sony Ericsson, for his help and knowledge in thermoplastic materials and *Engineering Calculation Specialist* Vijay Sharan, Sony Ericsson, who requested the project and made it happen.

Lund, August 2006

Fredrik Nordgren & Maria Nyquist

Abstract

There are high demands for improved material models today, both because of the capacity that today's computers provide and of economical reasons. The thesis assignment is to identify the mechanisms of the thermoplastic PC/ABS by performing experimental tests to which a suitable material model will be fitted. The choice of material model will be based on a thorough literature study. Material models used are restricted to existing models in Abaqus.

The mechanisms found in the experimental testing exhibits a highly complicated material. Behaviors like large strain elasticity, rate dependence, amplitude dependence, creep and damage are seen in the tensile tests.

In the investigation of material models the mechanisms found in the material and the current mechanical problems that Sony Ericsson are facing, e.g. high rate drop test simulations, are taken into consideration. A constitutive elasto-plastic viscoelastic model is presented. The model is implemented by an overlay method i.e. a combination of existing material models and verified in tensile and bending testing.

Contents

Chapter 1

Introduction

1.1 The company

Sony Ericsson is an outcome from the union between Ericsson and Sony Corporation witch took place in 2001. Ericsson contributed with great knowledge in telecommunications and Sony Corporations with their high skills concerning electronics. The combination of two well established and educated companies, along with a well formulated strategy that meets the costumer demands, has put Sony Ericsson in the lead position in the mobile communication industry.

Sony Ericsson is a genuine global company with approximately 5000 employees spread out all over the world. Originally all production, product design and development were located in Sweden but lately almost the entire production is moved to Asia where the manufacturing costs are considerably lower. The corporative management is located in London.

1.2 Thesis objective

The demands of low manufacturing costs and improved performance of products have lead to a stronger focus on virtual testing than physical testing. In simulations performed at Sony Ericsson it is important to include the specific behavior of plastics when simulating, for instance, drop tests.

Plastic materials are overall complicated materials due to their nonlinear behavior. It is relatively revolutionary to use plastic as a high toughness and impact tolerable material. This results in a poor documentation in literature. The interest for plastics in this field of application is on account of its low weight and low manufacturing costs. The treatment of cellular phones can be rather reckless compared to how we treat plastic products in general and are therefore demanding a high strength of the phone.

Today Sony Ericsson uses a viscoplastic material model based on linear elasticity which predicts the loading curve in a satisfying way. Due to the linear elasticity the model can not capture the Bauschinger-like unloading effect, which results in an overestimation of the remaining plastic strains.

Thereby, the thesis assignment is to identify the mechanisms of the material by performing experimental tests to which a suitable material model is fitted to. The choice of material model will be based on a thorough literature study. The model will be calibrated to experimental data and verified in Abaqus.

All results and material data in terms of stress and force levels have been normalized due to company secrecy policy.

1.3 Restrictions

The thesis is restricted to already existing models in Abaqus. Mainly because a Master thesis of this kind would need considerably more time to implement a user subroutine. Unfortunately there are few existing material models in Abaqus that deals with the complex behavior of thermoplastics. The experimental tests are limited to uniaxial tensile tests due to lack of equipment.

1.4 Methodology

The method used for this Master thesis is as following

- Literature study - Studies on different material models and research in the area. Also thermoplastics and testing methods are studied
- Experiments - Tensile testing, where mechanisms of the material are identified
- Model selection - Choice of material model based on literature study and experiments
- One-dimensional model - Model implemented in Matlab for parametric studies
- Model fitting and parameter calibration
- Verifications performed in Abaqus

Chapter 2

Thermoplastics

Thermoplastic are characterized by their reversible hardening process which makes them recyclable. Their structure contains long chains of monomers, a repeting group of polymer chains, that ensue from the polymerization process. Thermoplastics have in general the manufacturing advantage to be suited for injection molding and extrusion. They are also suited for addition of filling material to improve and change the mechanical properties. [1]

The characteristic look of the stress-strain curve of a plastic material is shown in Figure 2.1. As a result of experimental tests, behaviors like post-yield-strain softening a softening after the yield peak, which is due to the highly non-linear behavior of polymers under large deformations, rate dependency, Bauschinger-like unloading and creep are expected. [2]

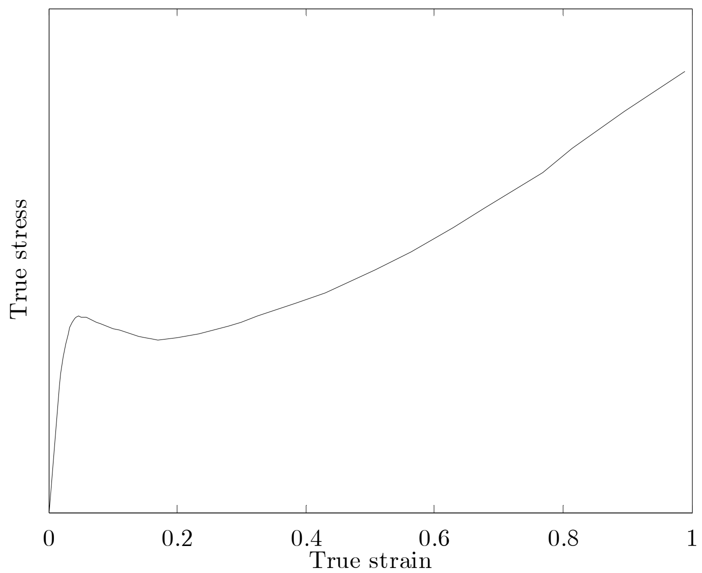

Figure 2.1: True stress-strain curve from tensile test [3]

2.1 History

Polymer blends have existed for quite some time though it was first during the 80's that it had its rapid growth of importance. The first patent of a polymer blend took place 1846 and as late as 1942 the first thermoplastic polymer blend where taken out patent for. The commercialization of a PC polymer took place year 1958. The first PC/ABS blend production started in year 1977 under the trade name Cycoloy. [4]

2.2 Mechanical Proporties

Polycarbonate (PC) is characterized for its high toughness, high modulus, flame resistance and high impact strength. The drawbacks of PC are high melt viscosity (difficult processability) and notch sensitivity. By blending various thermoplastics/thermoplastics elastomers together with PC these disadvantages can be eliminated.

Acrylonitrile-butadiene-styrene (ABS) is a rubber toughened thermoplastic that has properties such as good processability, notch insensitivity, and low cost. ABS plastic is used as a material for golf-ball covers, protective helmet and screw driver handle, etc. Another advantage is the relatively smooth surface finishes that easily can be decorated. Limitations of ABS are low thermal stability, and poor flame and chemical resistance. The addition of ABS minimizes the drawbacks of PC without removing other superior mechanical properties and also generates other useful properties, such as glossiness and low-temperature toughness. PC/ABS alloys are largest selling commercial polymer alloys in the world. [5][6]

2.3 Fillers

The primarily purpose of adding mineral fillers to polymers was to reduce the manufacturing costs. Today fillers play an increasingly functional role, such as improving the stiffness or surface finish of a polymer product. The reinforcement of thermoplastic compounds by short fibres has received special attention since it can be moulded into complex shapes and gives the composites good mechanical properties. In general, the stiffness and strength of the polymer matrix are enhanced by the addition of short fibres. [4][7]

Chapter 3

Constitutive modelling

3.1 Deformation of solids

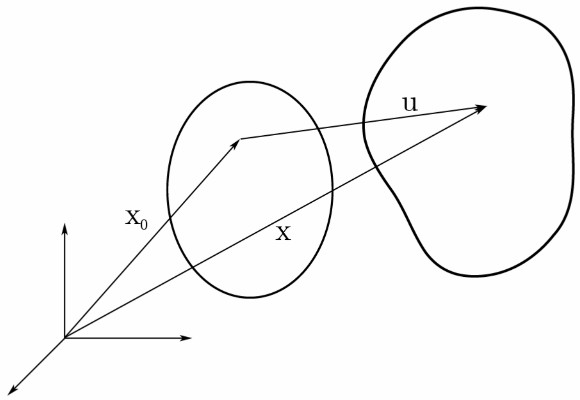

Figure 3.1: Displacement $\mathbf{u}$ from initial configuration $\mathbf{x}_0$ to current configuration $\mathbf{x}$.

Consider a material particle with an initial position $\mathbf{x}_0$. A displacement $\mathbf{u}$ gives the particle its current position [8]

$$\mathbf{x} = \mathbf{x}(\mathbf{x}_0) = \mathbf{x}_0 + \mathbf{u} \tag{3.1}$$

This description where the displacement is expressed in terms of the initial position is called a Lagrangian description. A line segment, $d\mathbf{x}_0$, in the neighbourhood of the point $\mathbf{x}_0$ can be mapped to the current domain with

$$d\mathbf{x} = \mathbf{F}\, d\mathbf{x}_0 \tag{3.2}$$

where F is the deformation gradient tensor with components

$$\mathbf{F} = \begin{bmatrix} \partial x_1 / \partial x_1^0 & \partial x_1 / \partial x_2^0 & \partial x_1 / \partial x_3^0 \\ \partial x_2 / \partial x_1^0 & \partial x_2 / \partial x_2^0 & \partial x_2 / \partial x_3^0 \\ \partial x_3 / \partial x_1^0 & \partial x_3 / \partial x_2^0 & \partial x_3 / \partial x_3^0 \end{bmatrix} \tag{3.3}$$

The deformation gradient tensor can be expressed in terms of the displacement gradient tensor as

$$\mathbf{F} = \mathbf{I} + \nabla\mathbf{u} \tag{3.4}$$

where $\mathbf{I}$ is the unit tensor and $\nabla\mathbf{u}$ is the displacement gradient tensor

$$\nabla\mathbf{u} = \begin{bmatrix} \partial u_1 / \partial x_1^0 & \partial u_1 / \partial x_2^0 & \partial u_1 / \partial x_3^0 \\ \partial u_2 / \partial x_1^0 & \partial u_2 / \partial x_2^0 & \partial u_2 / \partial x_3^0 \\ \partial u_3 / \partial x_1^0 & \partial u_3 / \partial x_2^0 & \partial u_3 / \partial x_3^0 \end{bmatrix} \tag{3.5}$$

3.2 Non-linear strain

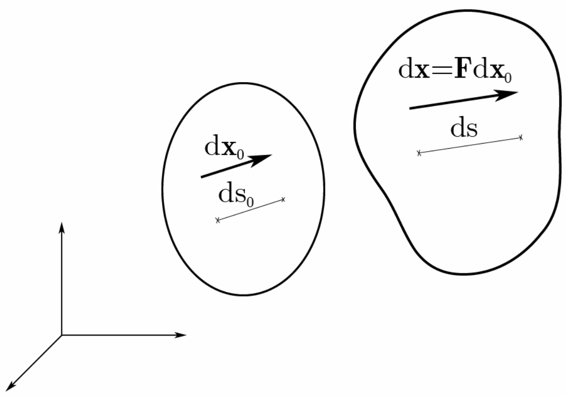

Figure 3.2: Motion of infinitesimal vector d$\mathbf{x}$

It is necessary to have a strain measure which characterizes the state of deformation at each point of the body. Green strain is a quadratic measure which, as all proper strain measures, is invariant to rigid body motions. Axial Green strain is defined as

$$\varepsilon_G = \frac{ds^2 - ds_0^2}{2\,ds_0^2} = \frac{d\mathbf{x}^T d\mathbf{x} - d\mathbf{x}_0^T d\mathbf{x}_0}{2\,ds_0^2} \tag{3.6}$$

where ds is the length of the vector $d\mathbf{x}$. Substitution of $d\mathbf{x}$ according to (3.2) gives the axial Green strain as

$$\varepsilon_G = \frac{d\mathbf{x}_0^T}{ds_0}\tfrac{1}{2}(\mathbf{F}^T\mathbf{F} - \mathbf{I})\frac{d\mathbf{x}_0}{ds_0} \tag{3.7}$$

The derivatives defines the direction and the Green strain tensor is defined as [9]

$$\mathbf{E} = \tfrac{1}{2}(\mathbf{F}^T\mathbf{F} - \mathbf{I}) = \tfrac{1}{2}(\nabla\mathbf{u} + \nabla\mathbf{u}^T) + \tfrac{1}{2}\nabla\mathbf{u}^T\nabla\mathbf{u} \tag{3.8}$$

Other important measures of deformation are the deformation tensor defined as

$$\mathbf{C} = \mathbf{F}^T\mathbf{F} \tag{3.9}$$

and the rate of deformation tensor also referred to as velocity strain

$$\mathbf{D} = \frac{1}{2}\left(\mathbf{L} + \mathbf{L}^T\right) \tag{3.10}$$

where $\mathbf{L}$ is the velocity gradient defined as

$$\mathbf{L} = \frac{\partial\mathbf{v}}{\partial\mathbf{x}} = (\nabla\mathbf{v})^T \tag{3.11}$$

3.3 Invariants

The principal invariants (I_1, I_2, I_3) of the right Cauchy-Green deformation tensor $\mathbf{C}$ are of great importance in elastic constitutive relations. They can be calculated from the eigenvalue problem

$$det\left(\mathbf{C} - \lambda^2\mathbf{I}\right) = 0 \tag{3.12}$$

with the solution

$$\begin{cases} I_1 = \lambda_1^2 + \lambda_2^2 + \lambda_3^2 \\ I_2 = \lambda_1^2\lambda_2^2 + \lambda_1^2\lambda_3^2 + \lambda_2^2\lambda_3^2 \\ I_3 = \lambda_1^2\lambda_2^2\lambda_3^2 \end{cases} \tag{3.13}$$

For simplicity, the volume change can be eliminated by writing the invariants on isochoric form $(\overline{I}_1, \overline{I}_2, \overline{I}_3)$ by defining the deformation gradient as

$$\overline{\mathbf{F}} = J^{-\frac{1}{3}}\mathbf{F} \tag{3.14}$$

where $J = \det(\mathbf{F})$ is the volume change.

3.4 Stresses

Another description required is the loading at an arbitrary point of the body. It is called the stress tensor and is, just like the strain tensor, a second order tensor. [9]

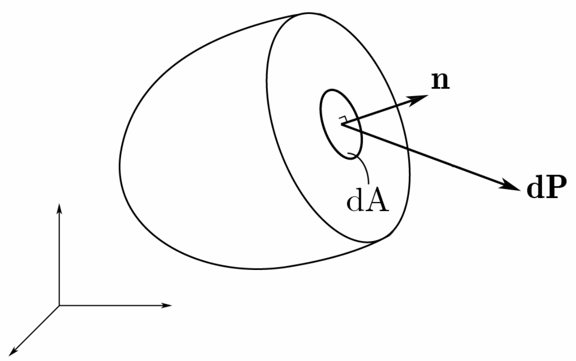

Figure 3.3: Force acting on a surface element

Consider a surface element dA of a loaded body illustrated in Figure 3.3. The surface can be external or internal i.e. a cross section of the body. The unit normal vector **n** represents the direction of the surface and the force vector **dP** acts on the surface element in the current configuration. The traction vector **t** on the surface is defined as

$$\mathbf{t} = \frac{\mathbf{dP}}{dA} \tag{3.15}$$

The traction vectors acting on the surfaces perpendicular to the coordinate axes (x_1, x_2, x_3) are denoted $\mathbf{t}_1, \mathbf{t}_2$ and $\mathbf{t}_3$ respectively with components as

$$\mathbf{t}_1 = \begin{bmatrix} \sigma_{11} \\ \sigma_{12} \\ \sigma_{13} \end{bmatrix} \qquad \mathbf{t}_2 = \begin{bmatrix} \sigma_{21} \\ \sigma_{22} \\ \sigma_{23} \end{bmatrix} \qquad \mathbf{t}_3 = \begin{bmatrix} \sigma_{31} \\ \sigma_{32} \\ \sigma_{33} \end{bmatrix} \tag{3.16}$$

where σ_{ij} are stress components. Components with equal indices are normal stresses and components with unequal indices are shear stresses. The stress tensor can be represented by a matrix in terms of the traction vectors and is defined as

$$\boldsymbol{\sigma} = \begin{bmatrix} \sigma_{11} & \sigma_{12} & \sigma_{13} \\ \sigma_{21} & \sigma_{22} & \sigma_{23} \\ \sigma_{31} & \sigma_{32} & \sigma_{33} \end{bmatrix} \tag{3.17}$$

By using moment equilibrium it can be proved to be symmetric, i.e.

$$\boldsymbol{\sigma} = \boldsymbol{\sigma}^T \tag{3.18}$$

The traction vector $\mathbf{t}$ can be calculated for an arbitrary direction $\mathbf{n}$ by using Cauchy's formula. The tensor $\boldsymbol{\sigma}$ is called the Cauchy stress tensor with components established in the current configuration and is therefore often referred to as true stress. In problems with large deformations, other stress measures can be defined in terms of the Cauchy stress. What differs these measures from the Cauchy stress is that they refer to other configurations. The first Piola-Kirchhoff stress is defined as

$$\mathbf{P} = J\,\boldsymbol{\sigma}\,\mathbf{F}^{-1} \tag{3.19}$$

The $\mathbf{P}$ tensor is not symmetric and its transpose is called the nominal stress. (In some literature, the nominal stress is denoted $\mathbf{P}$.) The second Piola-Kirchhoff stress is defined as

$$\mathbf{S} = J\,\mathbf{F}^{-1}\,\boldsymbol{\sigma}\,\mathbf{F}^{-T} \tag{3.20}$$

The transformation with $\mathbf{F}^{-1}$ makes the tensor symmetric and conjugate to the rate of Green strain. This makes the second Piola-Kirchhoff stress suitable for path-independent materials such as hyperelastic materials. The Cauchy stress tensor relates to the second Piola-Kirchhoff stress through the principle of virtual work as

$$\int_{V_0} \delta\mathbf{E}\,\mathbf{S}\,dV_0 = \int_V \delta\boldsymbol{\varepsilon}\,\boldsymbol{\sigma}\,dV \tag{3.21}$$

where the variation of the Green strain tensor can be expressed as

$$\delta\mathbf{E} = \tfrac{1}{2}(\mathbf{F}^T\delta\mathbf{D} + \delta\mathbf{D}^T\mathbf{F}) \tag{3.22}$$

and $\delta\boldsymbol{\varepsilon}$ is the variation of the logarithmic strain. The volumes are related by the Jacobian determinant $J = \det(\mathbf{F})$ as

$$dV = J\,dV_0 = \det(\mathbf{F})\,dV_0 \tag{3.23}$$

3.5 Elasticity

The characteristic of elastic strain is that the response is independent of the load history. After removing the load, the material returns to its initial condition and the unloading stress-strain curve retraces the loading curve, cf. Figure 3.4. [10]

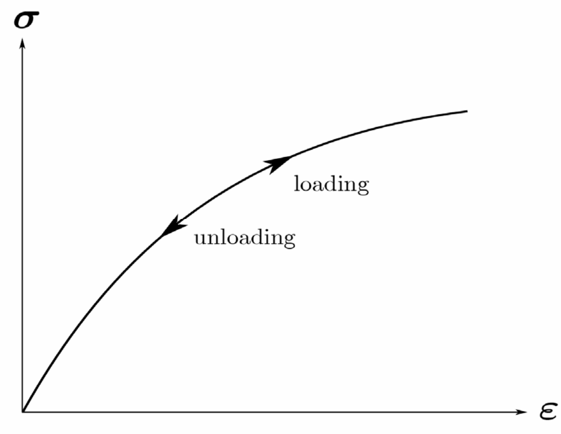

Figure 3.4: Elastic behavior

The elastic part of the stress-strain curve of most metals is linear. The stress is related to the strain by an elastic modulus which is constant through the elastic region. However, the elasticity of materials such as plastics and rubber shows a non-linear elastic behavior. Not only is the stress-strain curve non-linear, but the stress level is also dependent of the strain rate, cf. Figure 3.5.

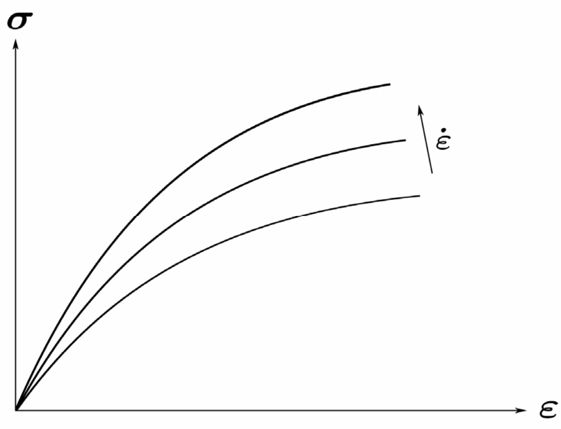

Figure 3.5: Strain rate dependence

3.5.1 Hyperelasticity

The stress-strain relationship of a hyperelastic material is derived from a stored strain energy function $W(I_1, I_2, I_3)$ based on strain invariants which makes the formulation frame-invariant. The existence of a stored energy function yields in a path-independent material. A general polynomial form of the strain energy function is [11]

$$W = \sum_{i+j=1}^{N} C_{ij}(\bar{I}_1 - 3)^i(\bar{I}_2 - 3)^j + \sum_{i=1}^{N} \frac{1}{D_i}(J-1)^{2i} \tag{3.24}$$

The simplest form is the Neo-Hookean which is an extension of Hooke's law to large deformations. It is only dependent of the first strain invariant and takes the form

$$W = C_{10}(\bar{I}_1 - 3) + \frac{1}{D_1}(J-1)^2 \tag{3.25}$$

The second Piola-Kirchhoff stress tensor for a hyperelastic material is given by

$$\mathbf{S} = 2\frac{\partial W}{\partial \mathbf{C}} \tag{3.26}$$

3.5.2 Viscoelasticity

In classical elasticity theory, according to Hooke's law, the stress is directly proportional to the strain amplitude and independent of the strain rate. Hydrodynamics, which deals with properties of viscous liquids, is described by Newton's law where the stress is directly proportional to the rate of strain, but independent of the strain amplitude. These laws are idealizations. However, the behavior of the solids and liquids approaches the laws for infinitesimal strains and strain rates, respectively.

The Maxwell model

Materials like polymers exhibit both a rate- and time-dependent as well as an amplitude dependent behavior known as viscoelasticity. A simple and linear representation of a viscoelastic material is the Maxwell model shown in Figure 3.6. It consists of a linear spring in series with a dashpot. The spring models the elasticity with stiffness $\boldsymbol{E}$ and the dashpot models the viscous response with viscosity $\boldsymbol{\eta}$. Such models are often referred to, especially in older literature, as rheological models where rheology means the science of viscous fluids. [12]

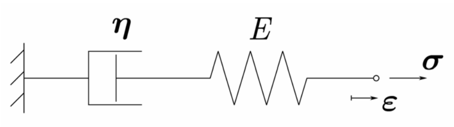

Figure 3.6: Maxwell element

The total strain in the element is the sum of the elastic and viscous strains and taking the derivatives of the strains gives

$$\dot{\varepsilon} = \dot{\varepsilon}^{e} + \dot{\varepsilon}^{v} \tag{3.27}$$

By using $\dot{\varepsilon}^{e} = \dot{\sigma} \,/\, E$ and $\dot{\varepsilon}^{v} = \sigma \,/\, \eta$, (3.27) can be written as

$$\dot{\sigma} + \frac{\sigma}{\tau} = E\dot{\varepsilon} \tag{3.28}$$

where $\tau = \eta \,/\, E$ is the relaxation time. A solution to (3.28) and consequently the viscoelastic stress response is given by the hereditary integral

$$\sigma(t) = \int_{-\infty}^{t} G(t-\tau)\frac{d\varepsilon(\tau)}{d\tau}\,d\tau \tag{3.29}$$

where $G(t) = E\, e^{-t/\tau}$ is the relaxation modulus.

The SLS model

A simple rheological model that behaves like a solid is the SLS (Standard Linear Solid) model which is a spring and a Maxwell element coupled in parallel, cf. Figure 3.7.

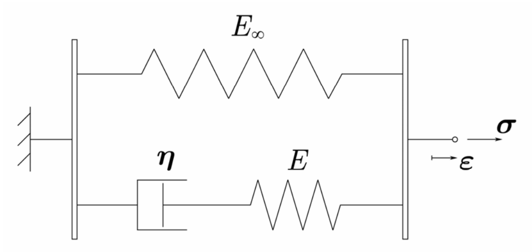

Figure 3.7: SLS model

The total stress is given by

$$\sigma = \sigma_\infty + \sigma_M \tag{3.30}$$

and the relaxation modulus for the SLS model is then

$$G(t) = E_\infty + E\, e^{-t/\tau} \tag{3.31}$$

The generalized Maxwell model

By adding more Maxwell elements in parallel, the properties of the SLS model is kept but with a better ability to fit the model to experimental data. This gives the generalized Maxwell model, cf. Figure 3.8.

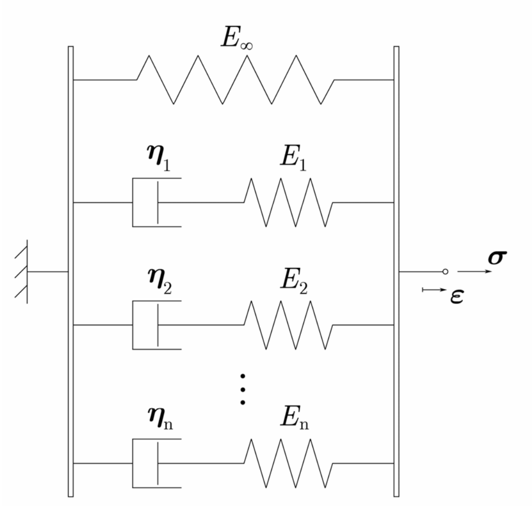

Figure 3.8: Generalized Maxwell model

The total stress in the generalized model is

$$\sigma = \sigma_{\infty} + \sigma_{M1} + \sigma_{M2} + \dots + \sigma_{Mn} \tag{3.32}$$

The relaxation modulus is the sum of all individual modulis and is given by a Prony series.

$$G(t) = E_{\infty} + \sum_{i=1}^{n} E_i \, e^{-t/\tau_i} \tag{3.33}$$

3.6 Creep

Creep is a time-dependent mechanism. One possibility to model the creep mechanism is to use a viscoelastic constitutive model.

There are three standard methods to determine the time-dependent behavior of a material, creep test, relaxation test and constant strain-rate test. When performing a creep test, the stress is kept constant and gives the strain versus time, cf. Figure 3.9. In the relaxation test, the strain is kept constant and gives the corresponding stress history, cf. Figure 3.10. The constant strain-rate test shows the rate dependent behavior of the material. A constant strain-rate is applied and the result is one stress-strain curve for each strain-rate, cf. Figure 3.11. [12]

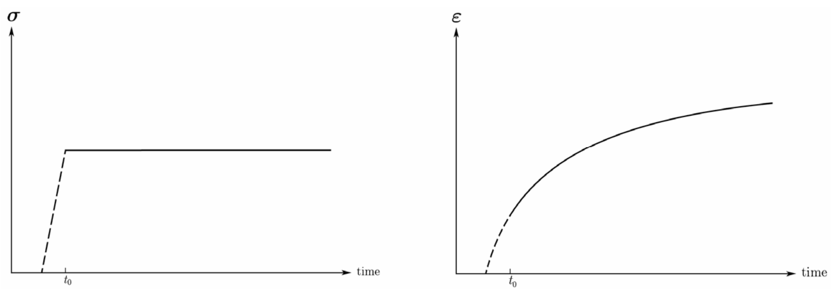

Figure 3.9: Creep test, stress with corresponding strain history

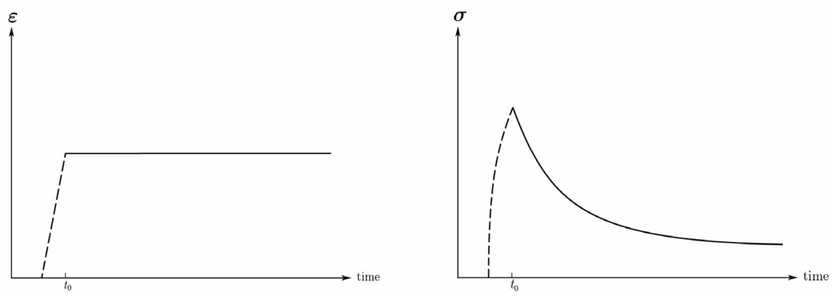

Figure 3.10: Relaxation test, strain with corresponding stress history

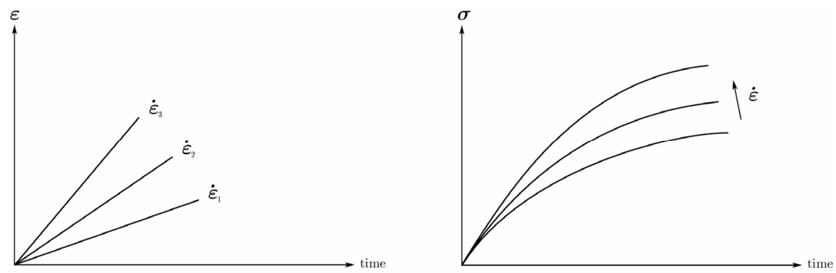

Figure 3.11: Strain rate test, different strain rates with corresponding stress response

3.7 Plasticity

At sufficiently high strain levels, most materials exhibit a non-linear behavior. This is often an irreversible process known as plasticity. Figure 3.12 shows a typical stress-strain relation from a tensile test on a metal bar for small deformations. [10]

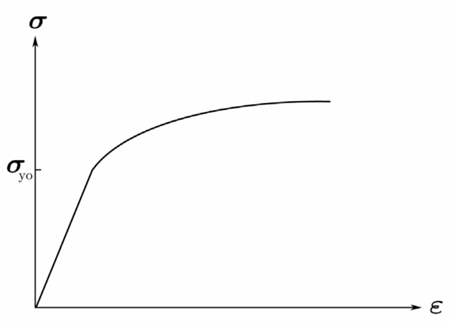

Figure 3.12: Plastic loading

The elastic limit is defined by a yield criterion and the plastic curve is governed by laws of hardening and a flow rule. The strains can be divided into an elastic part and a plastic part.

$$\varepsilon = \varepsilon^e + \varepsilon^p \tag{3.34}$$

When unloading in the plastic region, the behavior is again elastic. After complete unloading, the remaining strain is the plastic strain ε^p or damage in the material, cf. Figure 3.13. The stress level is not uniquely determined from the strain though it is dependent of the strain history.

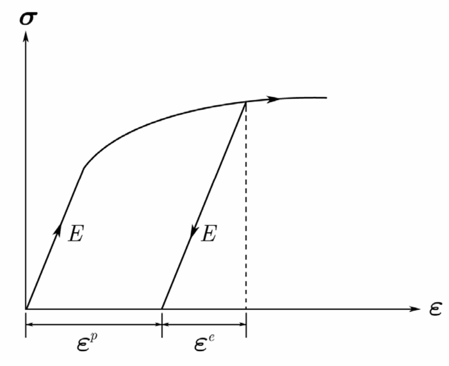

Figure 3.13: Plastic unloading

3.7.1 Yield criteria

In a given state, it has to be determined whether the response is elastic or plastic. For that reason the yield criteria is introduced as a yield surface.

$$f(\boldsymbol{\sigma}) = 0 \tag{3.35}$$

The function f is the yield function which defines a surface in the stress space. The idea of the surface is to divide the stress space into two parts. The inside where $f < 0$ is the elastic part and the surface where $f = 0$ is the plastic part. The stress cannot be outside the surface, only move it due to different hardening mechanisms. A common criteria used is the von Mises criterion which forms a circle in the deviatoric plane and a cylindrical surface in the stress space, cf. Figure 3.14. It is independent of hydrostatic stress and takes the form

$$\sqrt{3J_2} - \sigma_{y0} = 0 \tag{3.36}$$

where $J_2 = \frac{1}{2} s_{ij} s_{ji}$ is an invariant to the deviatoric stress tensor.

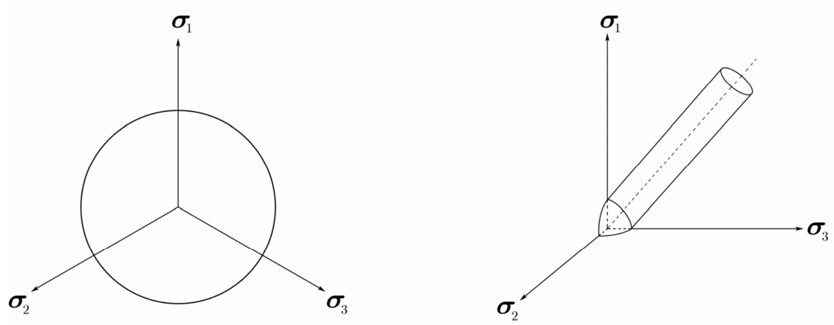

Figure 3.14: von Mises yield surface in the stress a) plane b) space

3.7.2 Hardening

The initial yield surface is described by

$$F(\boldsymbol{\sigma}) = 0 \tag{3.37}$$

During plastic loading the yield surface varies and the current yield surface can be expressed as

$$f(\boldsymbol{\sigma}, K^{\alpha}) = 0 \tag{3.38}$$

where $K^{\alpha}\,(\alpha = 1, 2, \ldots)$ are the hardening parameters. These parameters describe the changes in shape, size and position of the yield surface with plastic loading. The hardening parameters may change during plastic loading and internal variables κ^{α} are introduced so that

$$K^{\alpha} = K^{\alpha}(\kappa^{\alpha}) \tag{3.39}$$

Ideal plasticity

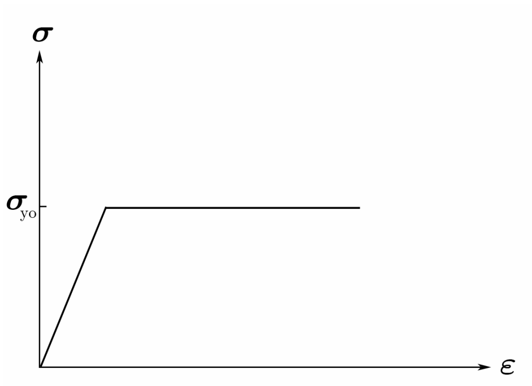

Figure 3.15: Ideal plasticity

The simplest case of plasticity is the ideal plasticity shown in Figure 3.15, which has no hardening effects. The yield surface remains fixed in the stress space and the non-existence of hardening parameters yields

$$f(\boldsymbol{\sigma}, K^{\alpha}) = F(\boldsymbol{\sigma}) = 0 \tag{3.40}$$

Isotropic hardening

A commonly used hardening model is the isotropic hardening in which the size of the yield surface changes whereas the shape and position remains unchanged. The current yield surface is then expressed in terms of the initial yield surface and a hardening parameter as

$$f(\boldsymbol{\sigma}, K^{\alpha}) = F(\boldsymbol{\sigma}) - K = 0 \tag{3.41}$$

Isotropic hardening of the von Mises criterion is shown in Figure 3.16.

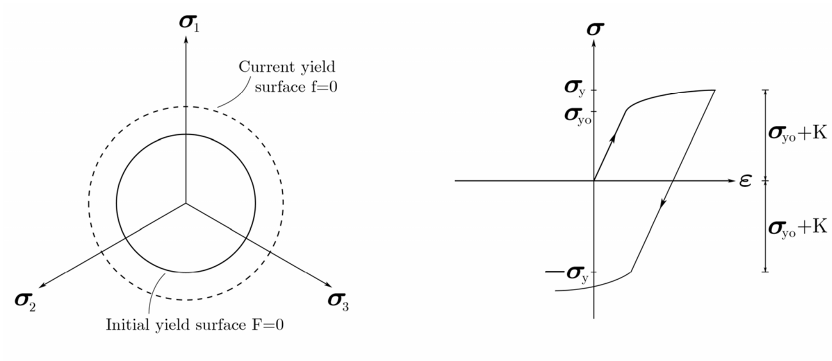

Figure 3.16: Isotropic hardening of the von Mises criterion

The current yield stress can be written as

$$\sigma_y = \sigma_{y0} + K \tag{3.42}$$

Figure 3.16 b) shows isotropic hardening during uniaxial loading. However, experiments show that many materials exhibit behavior where plasticity occurs earlier during the unloading than the isotropic hardening model predicts. This phenomenon is called the Bauschinger effect and is illustrated in Figure 3.17.

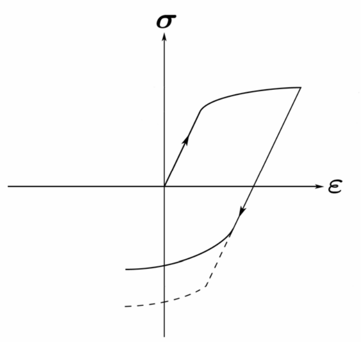

Figure 3.17: Bauschinger effect

Kinematic hardening

One way to approximate the Bauschinger effect is the Kinematic hardening illustrated in Figure 3.18.

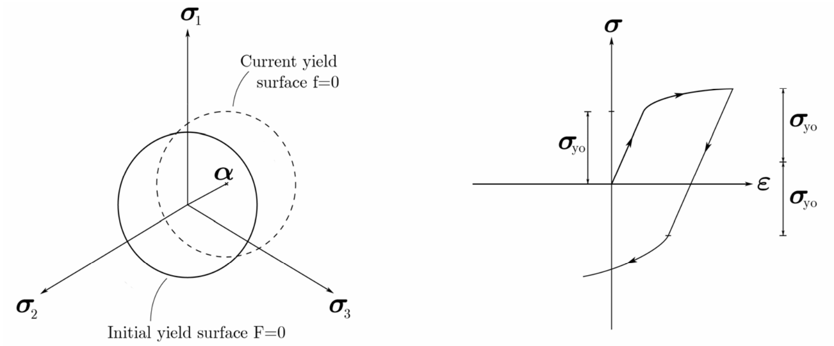

Figure 3.18: Kinematic hardening of the von Mises criterion

The size and the shape of the yield surface remains unchanged but the position of the surface changes during plastic loading. The model is a hardening model with an ability to move the center of the surface in the deviatoric stress plane. This movement is described by the parameter tensor $\boldsymbol{\alpha}$, also referred to as backstress. The initial value of the backstress is zero and hence, the initial yield surface coincides with isotropic hardening.

$$f(\boldsymbol{\sigma}, K^{\alpha}) = F(\boldsymbol{\sigma} - \boldsymbol{\alpha}) = 0 \tag{3.43}$$

3.7.3 Evolution laws

To identify the direction of the response, i.e. if it is plastic loading or elastic unloading, a criterion is needed.

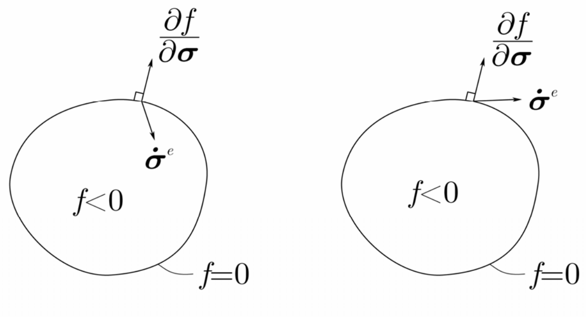

Figure 3.19: a) elastic unloading b) plastic loading

The scalar product of the outward normal to the yield surface and the direction of the stress gives the following loading-unloading condition.

$$\frac{\partial f}{\partial \boldsymbol{\sigma}}\dot{\boldsymbol{\sigma}}^{e} \begin{cases} < 0 \Rightarrow \textit{elastic unloading} \\ \geq 0 \Rightarrow \textit{plastic loading} \end{cases} \tag{3.44}$$

The increments in plastic strain are given by a flow rule. The simplest rule is the associated plasticity where the potential function chosen is the von Mises yield function. The evolution laws for incremental plastic strain is then given by

$$\dot{\boldsymbol{\varepsilon}}^{p} = \dot{\lambda}\frac{\partial f}{\partial \boldsymbol{\sigma}} \tag{3.45}$$

$$\dot{\kappa}^{\alpha} = -\dot{\lambda}\frac{\partial f}{\partial K} \tag{3.46}$$

where $\dot{\lambda}$ is the plastic multiplier which can be derived by using the so-called consistency relation. During plastic loading, the stress point remains on the yield surface, i.e. $f = 0$. This gives the consistency relation

$$\dot{f} = 0 \tag{3.47}$$

With a given plastic multiplier, the effective plastic strain is defined as

$$\dot{\varepsilon}_{eff}^{p} = \sqrt{\frac{2}{3}\dot{\varepsilon}^{p}\dot{\varepsilon}^{p}} \tag{3.48}$$

For von Mises plasticity it can be shown that $\dot{\varepsilon}_{eff}^{p} = \dot{\lambda}$.

3.7.4 Plasticity for large deformations

In plasticity for large deformations, it is not possible to make a decomposition of the strain tensor like the additive decomposition of $\boldsymbol{\varepsilon}$ in small strain plasticity. A common method that also is used by Abaqus is the additive split of the rate of deformation tensor [11]

$$\mathbf{D} = \mathbf{D}^{e} + \mathbf{D}^{p} \tag{3.49}$$

which splits the rate of deformation tensor into an elastic and a plastic part. It is now suitable to use a constitutive relation on rate form, which means that the elasto-plastic models are based on hypoelasticity. The objective rate of stress can be expressed as

$$\boldsymbol{\sigma}^{\nabla} = \mathbf{D}^{const} : \mathbf{D}^{e} \tag{3.50}$$

where $\mathbf{D}^{const}$ is the elastic constitutive stiffness tensor. To obtain the total stress it is necessary to integrate the stress rate.

3.8 Constitutive modelling of polymers

During the past twenty years, the research in constitutive modelling of polymers has increased significantly. However, a suitable model for thermoplastics is yet to be implemented by the commercial FE-codes, e.g. Abaqus. A desired model would be able to capture all the different mechanisms in the material such as large strain elasticity, rate dependence, amplitude dependence, creep and damage. Many different models have been proposed in the research where these, or some of these, effects can be captured in order to model the material in a satisfying way. Much of the research has been on elastomers and thermoplastics used for medical implants in e.g. joint replacements.

Much of the early work on plastic deformation of amorphous polymers was done by Boyce, Parks, Argon and Arruda [8][14] which i.e. resulted in the Arruda-Boyce model. It is a model based on a multiplicative decomposition of the deformation gradient into one elastic part $\mathbf{F}^{e}$ and one plastic part $\mathbf{F}^{p}$, i.e.

$$\mathbf{F} = \mathbf{F}^{e}\mathbf{F}^{p} \tag{3.51}$$

The stress state is then related to the elastic part of the deformation gradient, which can bee seen as a map between the current configuration and an introduced stress free intermediate configuration. Since the stress, in contrast to the hypoelastic formulation in (3.50), can be calculated from the total elastic deformation (via $\mathbf{F}^{e}$) it is possible to base the elasto-plastic model on hyperelasticity. In one dimension, the model can be thought of as a linear elastic spring in series with a parallel arrangement of a viscoplastic dashpot and a non-linear hardening spring. In [2], tensile tests on polycarbonate (PC) was made and modelled in Abaqus with the Arruda-Boyce model. A method for obtaining the true stress-strain curve after necking in tensile testing is also presented. Other models, based on the same theory, was proposed by Wu and van der Giessen [15] and later (2003) by Anand and Gurtin [16]. All these models can capture the large deformation elastic-viscoplastic response of amorphous polymers but they cannot account for the small strain (<30%) viscoelasticity and the Bauschinger-type unloading.

Hassan and Boyce [17] studied the nonlinear viscoelastic viscoplastic behavior of amorphous polymers in the small strain region. They also formulated a one-dimensional constitutive model which took account of the free-volume, i.e. the molecular-packing irregularities. The model captures the creep and Bauschinger-type unloading effect as well as the strain-hardening/softening of polymers.

Anand and Ames [18] have recently (2006) developed a new three-dimensional, internal variable, model for the viscoelastic-plastic deformation of amorphous polymers. The model is based on a generalized Kelvin-Voigt model which is a classical linear viscoelastic model. This is, however, an extension to linear theory that works in the nonlinear finite deformation range. The model was implemented in Abaqus/Explicit as a user material subroutine with satisfying results in terms of creep, unloading, the post-yield softening as well as cyclic loading.

An older (1987) model based on hyperelasticity was proposed by Simo [19] which combines hyperelasticity with damage effects. Models that combine the elastic-viscoelastic-elastoplastic behaviors have been proposed by Miehe and Keck [20] and Lin and Schomburg [21]. A way of implementing an elastic-viscoelastic-elastoplastic model in commercial software (with existing models) by an overlay of meshes was proposed by Austrell and Olsson [22]. The method was used for modelling of elastomers and will be used in this thesis.

3.8.1 The Overlay Method

The rather complex behavior of thermoplastics, with both rate and amplitude dependence, can be modelled by combining a generalized Maxwell model with an elasto-plastic model. The elasto-plastic model in Abaqus is based on hypoelasticity and not on the same hyperelasticity as the viscoelastic and elastic models are, as would be preferred. A one-dimensional representation of the viscoelastic-elastoplastic model is a generalized Maxwell model and a simple Coulomb frictional element coupled in parallel, c.f. Figure 3.20.

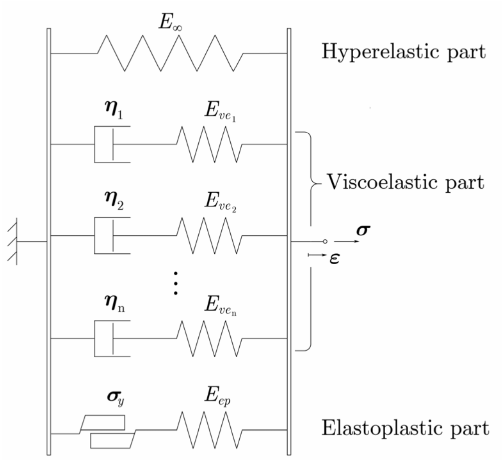

Figure 3.20: One-dimensional representation of proposed constitutive model

The total stress can be obtained as a summation of the stress tensors from the different elements as

$$\boldsymbol{\sigma} = \boldsymbol{\sigma}^{e} + \boldsymbol{\sigma}^{ve} + \boldsymbol{\sigma}^{ep} = \boldsymbol{\sigma}^{e} + \sum_{i=1}^{n} \boldsymbol{\sigma}_i^{ve} + \boldsymbol{\sigma}^{ep} \tag{3.52}$$

To implement this model in a commercial FE-code, without writing a user material subroutine, an overlay of finite element meshes is required. Different stresses will then be obtained from the separate models and the total stress is, as in one dimension, the sum of the individual stress tensors. The same topology is used for the different models, i.e. multiple elements are connecting the same nodes. In Abaqus, both hyperelasticity and viscoelasticity can be modelled by a single model. The viscoelasticity is implemented based on a Prony series and therefore, the first two models can be modelled as one. The principle of the overlay method is shown in Figure 3.21.

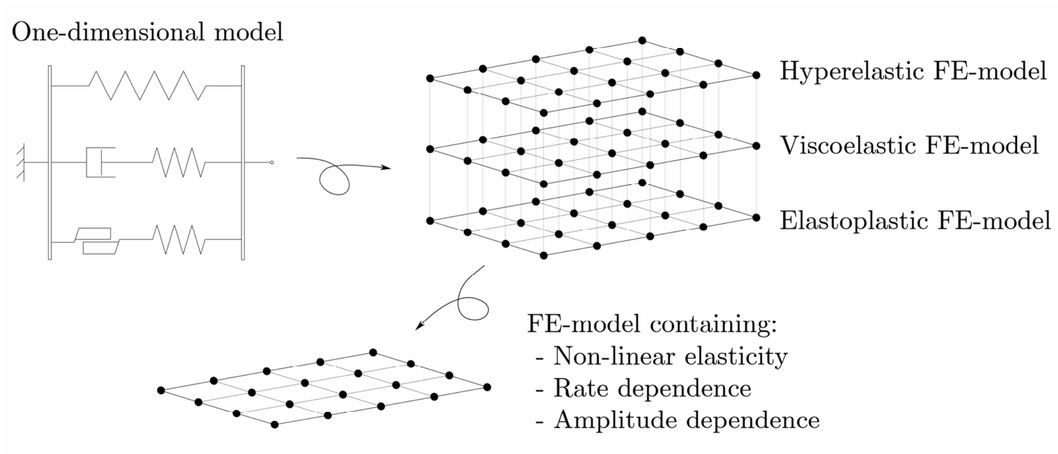

Figure 3.21: Principle of the overlay method

The material parameters in the model can be fitted in one dimension from tensile testing and then simply be copied to three dimensions. For that reason, a one-dimensional model has been implemented in Matlab.

Chapter 4

Experiments

There is a need to perform material tests to better understand the behavior of materials. The equipment used is a tensile test machine from Sony Ericsson's laboratory. The first set of tests is tensile tests performed at different loading rates and with the same unloading rate at 1 kN/s. These tests will show the rate dependence and recovery of the material. Another set of tests will be performed at the same loading rate, drawn to different strain levels. This test will also show the degree of viscosity and plasticity. In the last tensile tests, the specimen will be drawn to 8 mm, before necking. At specific values of the force the unloading will be held constant to investigate the recovery and creep.

An additional bending test is performed in order to verify the constitutive model in a different state of stress. Bending is the most usual type of deformation in a drop test simulation where both tensile and compressive strains occur.

4.1 The tensile test

The specimen dimensions follow the norm ISO 527-2/1A and are shown in Figure 4.1.

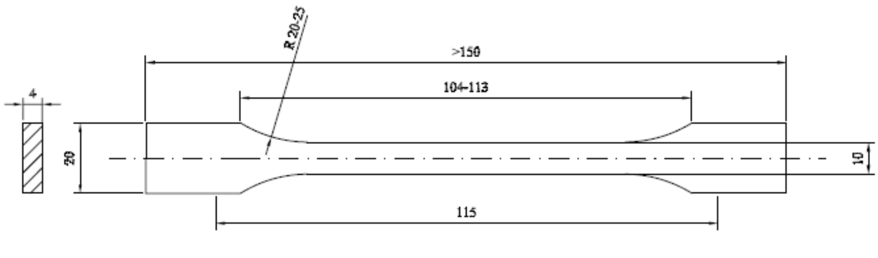

Figure 4.1: The dimensions of the specimen

4.1.1 The stress-strain curve

Performing tensile test for sufficiently small deformations, the difference between the current and the original geometries are negligible. In thermoplastics large deformations are rapidly achieved with applied force and a nonlinear application is needed. The measuring procedure works as following. The stretch is defined as [9]

$$\lambda = \frac{L}{L_0} \qquad \text{and} \quad L = L_0 + \delta \tag{4.1}$$

L is the length of the gage section and δ is the elongation. The engineering strain is given by

$$\varepsilon_0 = \frac{\delta}{L_0} = \lambda - 1 \tag{4.2}$$

The nominal stress is defined as

$$\sigma_0 = \frac{F}{A_0} \tag{4.3}$$

where F is the force and A_0 is the cross-sectional area. Since the geometrical changes has to be taken to consideration, true stress is defined as

$$\sigma = \frac{F}{A} \tag{4.4}$$

where A is the current-sectional area. The true strain or the logarithmic strain can be measured by integrating the change of unit current length.

$$\varepsilon = \int_{L_0}^{L} \frac{1}{L} dL = \ln\left(\frac{L}{L_0}\right) = \ln(\lambda) \tag{4.5}$$

The material time derivative of the above expression leads to following expression in the one dimensional case. The logarithmic strain is equal to the rate of deformation

$$\dot{\varepsilon} = \frac{\dot{\lambda}}{\lambda} = D_{11} \tag{4.6}$$

To generate true stress the cross-sectional area needs as a function of the deformation. The Jacobian acts as reference to current volumes. When the material is incompressible the Jacobian is set to 1. [14]

$$A = \frac{JA_0L_0}{L} = \frac{JA_0}{\lambda} \tag{4.7}$$

The Cauchy stress is defined as

$$\sigma = \frac{F}{A} = \lambda \frac{F}{JA_0} = \lambda J^{-1}\sigma_0 \tag{4.8}$$

4.1.2 Plastic Behavior

When performing a uniaxial tension test, most polymers begin to deform inhomogeneously at relatively small strains. This process is called necking and usually starts before the softening according to the stress- strain curve. In the initiation of necking a collection of sheer zones occurs rapidly and generally at the peak load or nominal yield stress. Since the stress state is difficult to define as well as the strain and strain rate vary appreciably over the gauge section the neck complicates measurements of material properties. The neck stabilises after the shallow load minimum and the deformation continue to propagate with relatively constant force and with some creep-like response within the material. With continuous of strain the softening process will lead to a hardening process until failure. [2][23][24]

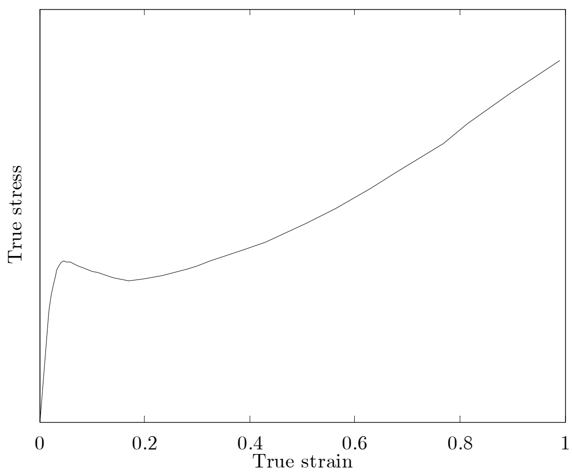

Figure 4.2: The true stress – strain curve for PC/ABS [3]

4.1.3 Geometric tensile instability

At large deformations, the test specimen itself is unstable due to the Poisson effect which causes a significant reduction in cross-section area. The force is then resisted over a reduced area which leads to an increase in stress and strain and ultimately to instability. This effect can occur, not only by softening plasticity, but also in a purely elastic material.

4.1.4 Factors of impact on experimental tests

It is proven that thickness influences the stress state within the material. For instance crazing (unstable local plastic deformation) occurs easier in a thick notch plate because of the more severe strain stress state ahead of the notch in the material. In a thinner plate the stress state is of lower concentration and can become plane stress. Since deformation is easier under plane stress conditions more energy can be absorbed by the material. Even though PC is a tough material it shows brittle behavior in thick-walled applications. [25]

4.1.5 Data from material supplier

The data given from the material supplier are information from tensile tests taken at different strain rates. The tensile test curves in Figure 4.3 show the results for an interval of strain rates between 0.000073 and 1.0 s^{-1}.

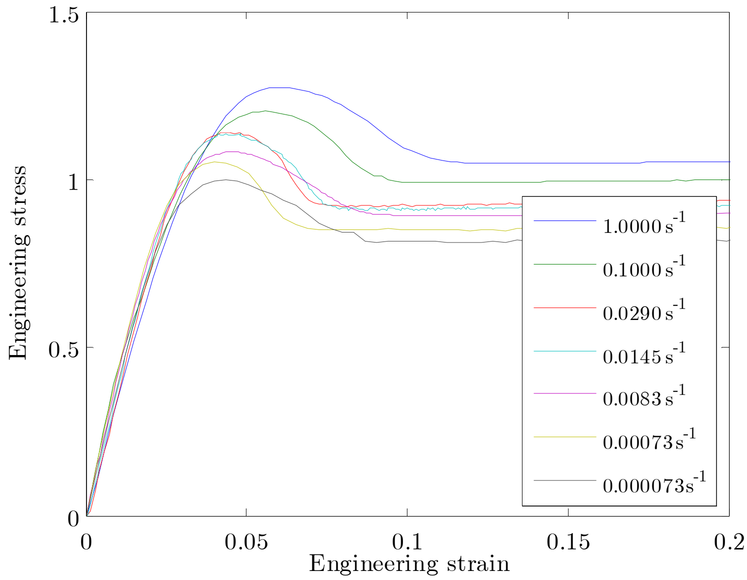

Figure 4.3: Tensile test data for PC/ABS [26]

Since most simulations are performed for even higher rates. A drop test is calculated to reach about 20% strain and is simulated during 1 ms which corresponds to a strain rate of 200 s^{-1}. Following procedure is done to estimate an engineering stress- strain curve for higher rates then from experiments and material supplier. The maximum engineering stresses for each tensile test i.e. Figure 4.3 are plotted and the values are shown in Table 4.1

Table 4.1: Maximum engineering stresses for different strain rates

$\dot{\varepsilon}$ (s^{-1})	σ_{max} (Rel.)
0.000073	1.00
0.00073	1.05
0.0083	1.08
0.0145	1.13
0.0290	1.13
0.1000	1.20
1.0000	1.27

In Figure 4.4 a) the maximum engineering stress values show a typical logarithmical appearance. In Figure 4.4 b) the maximum values are plotted with a logarithmical scale. By performing a least square method the values become a linear function.

a)

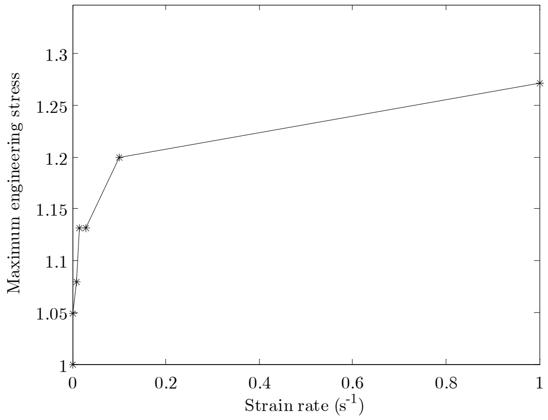

b)

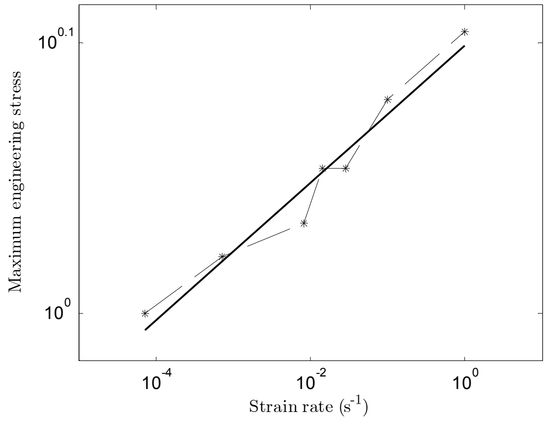

Figure 4.4: a) Maximum engineering stress values from tensile tests versus experiment strain rate b) Logarithmical maximum engineering stress values and a linear function fitted with the least square method

Using the linear function a high rate curve is estimated by extrapolating the curve from a given engineering stress-strain curve with the highest rate c.f. Figure 4.5.

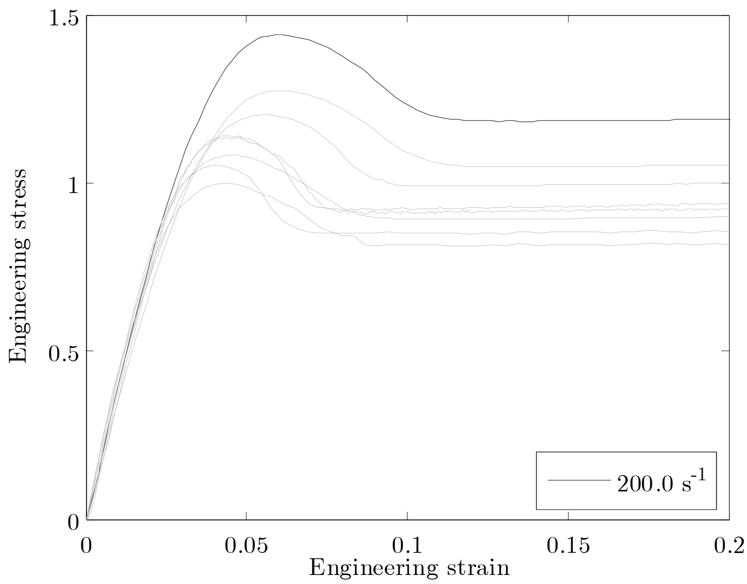

Figure 4.5: Estimated engineering stress-strain curve for 200 s^{-1}

4.2 Bending test

To be able to perform the bending test the test equipment had to be designed and the manufacturing was done in the Sony Ericsson workshop. The method used is similar to ISO 178, a method for determination of flexural properties of rigid plastics, but with modifications so that the specimen can be plastically deformed, c.f. Figure 4.6. The specimen is supported by bearings so that friction in the contact region can be eliminated. Force or displacement is applied by a probe, linked by a gauge to the tensile machine.

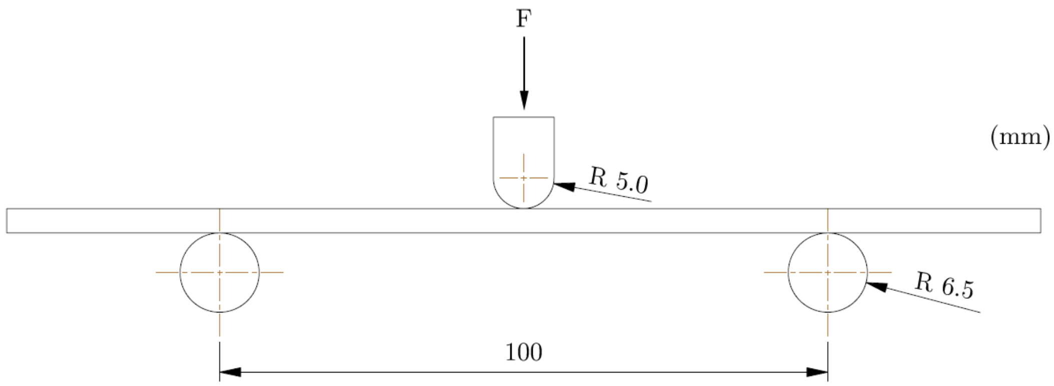

Figure 4.6: Bending test setup

The edges are removed to get a geometry which will perform better in the bending test set up. The rectangular geometry of the specimen is shown in Figure 4.7.

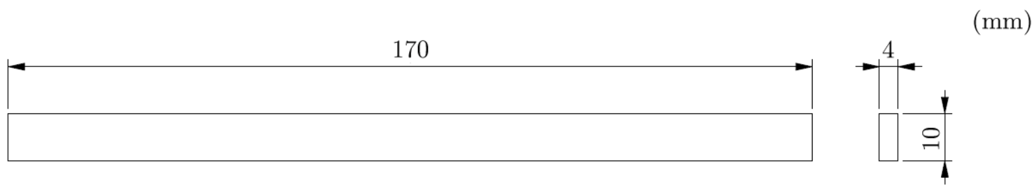

Figure 4.7: The geometry of the bending test specimen

4.3 Results

4.3.1 Tensile tests

Loading and unloading with different strain rates

Demonstrated in fig Figure 4.8 the material behaves linearly up till about 3% (3.5 mm) straining were the material introduces non-linear behavior. The yield stress is located at about 5% (5.7 mm) strain where a post-yield softening occurs. These specimens are drawn to approximately 7% (8 mm) strain, which is slightly before necking and the change in the cross-sectional area. The experiments performed with high rates reach a higher maximum stress and seem to have little remaining plastic deformations after unloading. Tests performed with lower rates results with more plastic deformation. The material shows an obvious rate dependence in the non-linear region in both loading and unloading. Every curve represents a separate specimen. The test at the lowest rate, i.e. 0.5 mm/min is considered static.

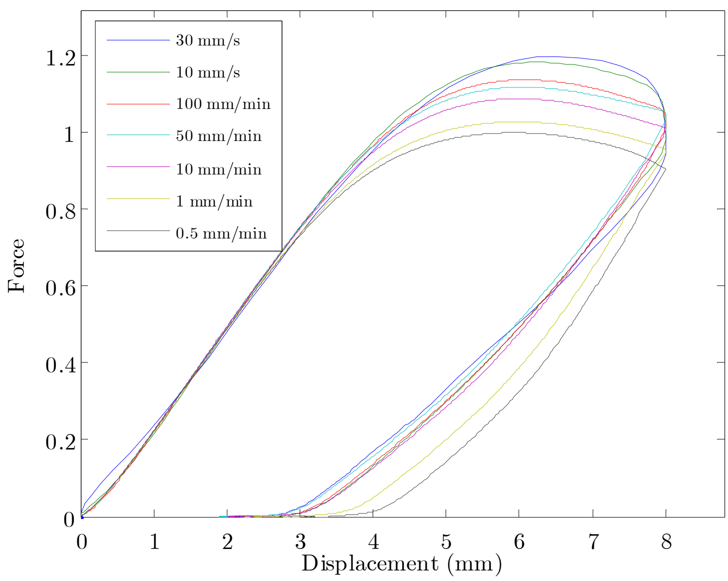

Figure 4.8 Loading at different strain rates and unloading at 1 kN/s

The recovery of the material in Figure 4.9 shows that the specimens at high rates recover more.

Necking is a plastic deformation caused by shear yielding and therefore leads to poorer recovery. Since the specimens are strained to before introduction of necking the material stays fairly elastic and most of the recovery occurs quickly when load is released. Most of the recovery happens in a few seconds. The curves represent the entire unloading including 60 s of recovery when the unloading has ended. Further ahead it is explained why a recovery of 60 s is chosen.

For the curves in Figure 4.9 the origin is defined as the start point of the unloading.

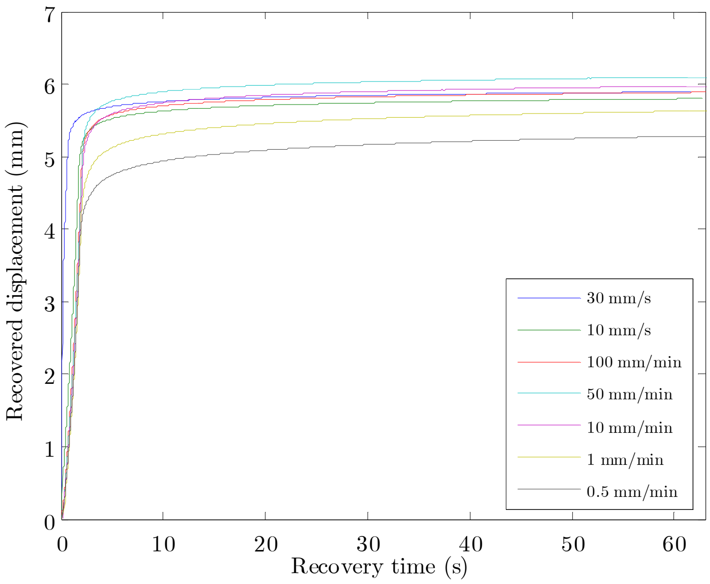

Figure 4.9: Unloading and recovery (60 s) of the material

As a supplemented test three specimens were strained to 7% (8 mm). The unloading is interrupted and held at 0.5, 0.25 and 0 force to investigate the recovery of the material. The x in Figure 4.10 indicates the location after 1 hour of recovery. When held at 0.25 the material recovered similarly to the recovery at 0. The recovery at 0.5 is less and a likely assumption is that the recovery becomes even more less when held at a higher load. At a certain force value the recovery effect will be smaller then the creep and the displacement would increase instead.

As a consequence of the applied force acting on the specimen, the material is let to recover for longer time, i.e. 1 hour instead of 60 s, since the applied force can affect the recovery process.

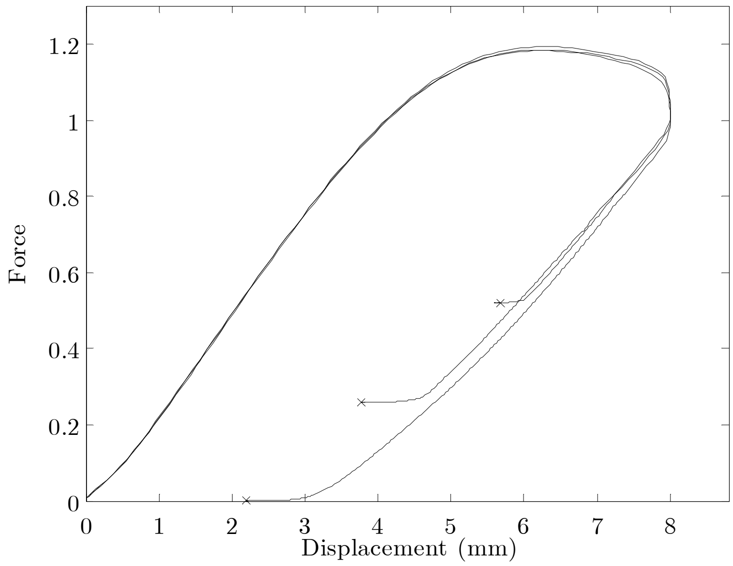

Figure 4.10: Recovery after 1 hour when held at 0.5, 0.25 and 0 force

Loading and unloading to different strain levels

Each curve in Figure 4.11 represents a separate specimen. The specimens are extended to different strain levels according to the curves. The loading rate is 10 mm/s and the unloading rate is 1 kN/s. The test is then held for 60 s at zero load and the material is let to recover. The recovered displacement is shown in Figure 4.12. The curves show the entire unloading from maximal displacement.

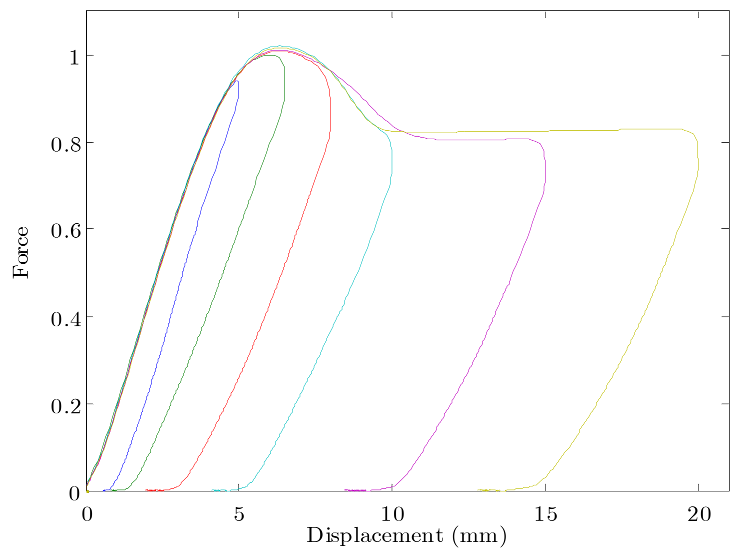

Figure 4.11: Loading at 10 mm/s and unloading at 1kN/s to different strain levels

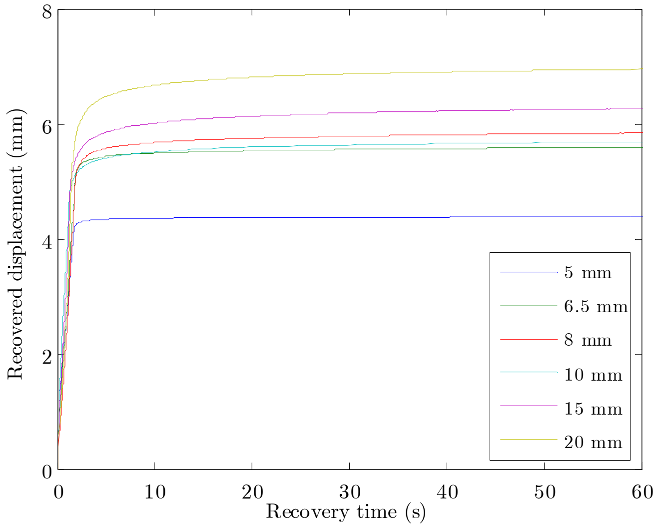

Figure 4.12 Unloading and revovery (60 s) of the material

In Figure 4.13 a) the total unloading procedure including recovery is shown for a specimen drawn to 10 mm. The unloading rate is 1 kN/s . Figure b) shows the recovery of the material when the unloading is completed and the force has reached 0 N. The dotted lines show the recovered displacement after 1 and 15 hours respectively. Most of the recovery occurs during the first 10 seconds and after 60 s the gradient of the curve is fairly small. The material does not recover much more after 1 or 15 hours than it does in 60 s. Letting the specimens recover for more than 60 s would therefore not give further profitable information.

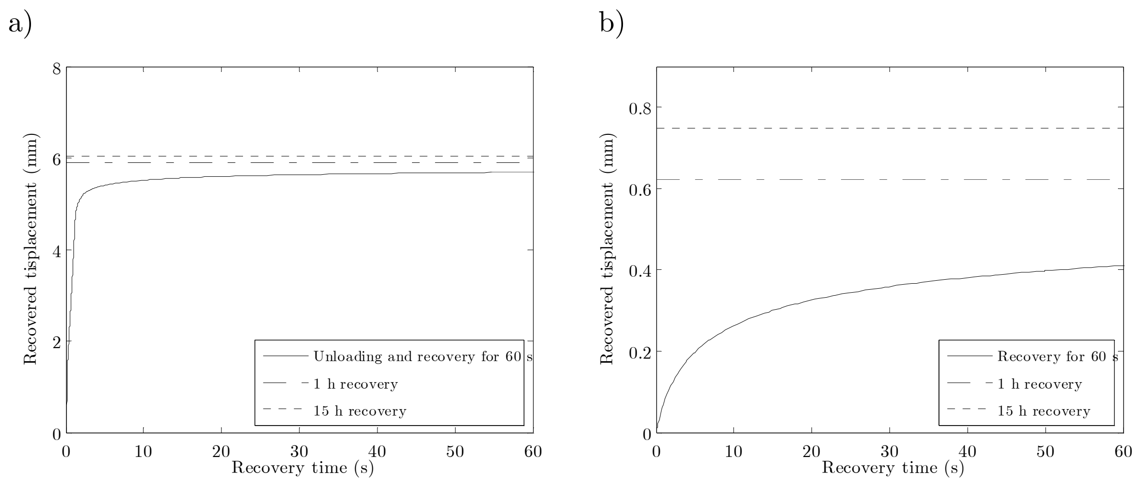

Figure 4.13: Loading at 10 mm/s to 10 mm and unloading at 1 kN/s. Recovery for 60 s, at 1 h and 15 h a) Unloading and recovery b) Recovery; from F = 0 N

4.3.2 Bending test

Two sets of bending tests where performed at downward vertical rates of 4 mm/min and 20 mm/s. The lower rate corresponds to the strain rates for the static tensile test. The specimens where bended down to 10, 20, 30 and 40 mm c.f. Figure 4.14 and Figure 4.15. The tests where all unloaded at 20 N/s and left for recovery for 5 min. The x in the figures indicates the location after 5 min of recovery.

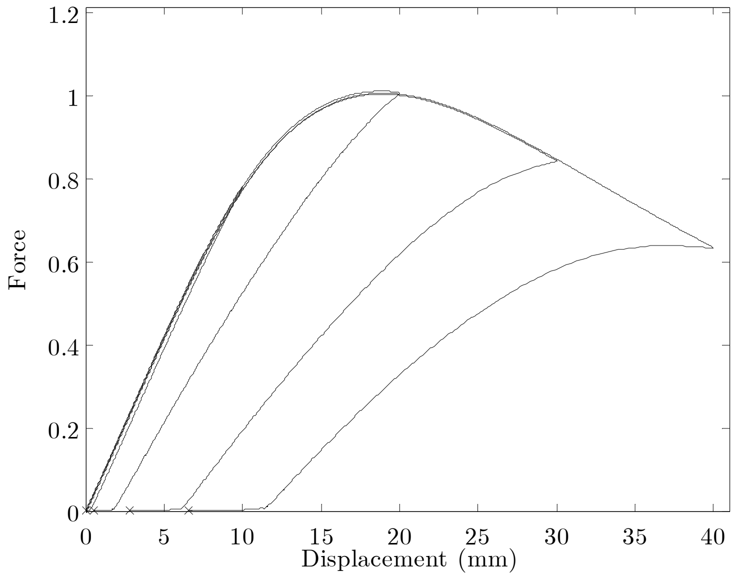

Figure 4.14: Bending tests at 0.06667 mm/s and unloaded at 20 kN/s

The specimen bended to 10 mm does not begin to deform plastically and follow the loading curve when unloaded. The maximum force for the static test tests reached 70 N while for the dynamic tests reached a maximum force of 79 N.

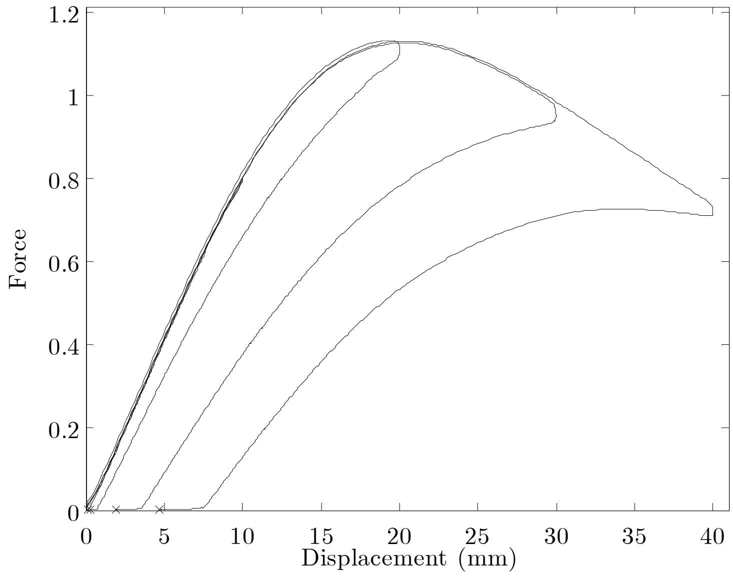

Figure 4.15: Bending tests at 20 mm/s s and unloaded at 20 kN/s

4.4 Discussion

It is desirable to run the tests at considerably higher rates but the equipment is limited to a maximum rate of 33 mm/s. The fastest tests are run at a rate of 30 mm/s. Material data supplier has contributed with tensile tests at higher strain rates but these do not include unloading information.

Looking closer at the beginning of the tensile tests one can distinguish a slight bend in the curve. This was due to the fact that the grips in the testing machine were, in the beginning of the test, pushed further into the material with increasing force with a false displacement as a result. The displacement data were therefore moved 0.18 mm to the left for the material model calibrations.

Chapter 5

A study of strain energy functions

A parametric study of different strain energy functions for hyperelasticity has been performed. The purpose of the study is to investigate the properties of the different functions and their capabilities to capture the polymeric behavior. The models are fitted to a true stress-strain curve from a tensile test on PC/ABS. Abaqus has a built-in function for fitting of hyperelastic constants to experimental test data which has been used.

The strain energy functions investigated are Neo-Hooke, Mooney-Rivlin, Ogden and the Polynomial form which can be fitted up to the order of two. When fitting the constants, full incompressibility is assumed. [11]

5.1 Theory

5.1.1 Strain energy functions

The strain energy functions are, for uniaxial mode, given in terms of a principal stretch $\lambda_U = 1 + \varepsilon$. The first two strain invariants for uniaxial loading are

$$\begin{cases} I_1 = \dfrac{2}{\lambda} + \lambda^2 \\ I_2 = \dfrac{1}{\lambda^2} + 2\lambda \end{cases} \tag{5.1}$$

The nominal stress-strain relationship for an arbitrary stored strain energy function $W(I_1, I_2)$ can now be derived by using the principle of virtual work and it follows that

$$\sigma = \frac{\partial W}{\partial \lambda_U} = \frac{\partial W}{\partial I_1}\frac{\partial I_1}{\partial \lambda_U} + \frac{\partial W}{\partial I_2}\frac{\partial I_2}{\partial \lambda_U} \tag{5.2}$$

The different strain energy functions evaluated are presented in Box 5.1.

Box 5.1: Strain energy functions

Neo-Hooke:

$$W = C_{10}(\bar{I}_1 - 3) + \frac{1}{D_1}(J_{el} - 1)^2 \tag{5.3}$$

Mooney-Rivlin:

$$W = C_{10}(\bar{I}_1 - 3) + C_{01}(\bar{I}_2 - 3) + \frac{1}{D_1}(J_{el} - 1)^2 \tag{5.4}$$

Ogden:

$$W = \sum_{i=1}^{N} \frac{2\mu_i}{\alpha_i^2}(\bar{\lambda}_1^{\alpha_i} + \bar{\lambda}_2^{\alpha_i} + \bar{\lambda}_3^{\alpha_i} - 3) + \sum_{i=1}^{N} \frac{1}{D_i}(J_{el} - 1)^{2i} \tag{5.5}$$

Polynomial (N=2):

$$\begin{aligned} W &= C_{10}(\bar{I}_1 - 3) + C_{01}(\bar{I}_2 - 3) + C_{20}(\bar{I}_1 - 3)^2 \\ &+ C_{11}(\bar{I}_1 - 3)(\bar{I}_2 - 3) + C_{02}(\bar{I}_2 - 3)^2 + \frac{1}{D_1}(J_{el} - 1)^2 \end{aligned} \tag{5.6}$$

5.1.2 Compressibility

At small strains, thermoplastics are compressible and almost incompressible at larger strains (i.e. after yielding). However, in Abaqus/Explicit, it is not possible to assume a fully incompressible material. The relative compressibility of a material can be expressed in terms of its initial bulk modulus K_0 to its initial shear modulus μ_0. It can also be expressed in terms of Poisson's ratio as

$$\nu = \frac{3K_0 / \mu - 2}{6K_0 / \mu + 2} \tag{5.7}$$

By specifying the Poisson's ratio, the initial bulk modulus can then be calculated as

$$D_1 = \frac{2}{K_0} = \frac{3(1 - 2\nu)}{\mu_0(1 + \nu)} \tag{5.8}$$

The initial shear modulus can be calculated from

$$\mu_0 = 2(C_{10} + C_{01}) \tag{5.9}$$

for the Polynomial form and

$$\mu_0 = \sum_{i=1}^{N} \mu_i \tag{5.10}$$

for the Ogden form.

5.1.3 Fitting procedure

From the experimental data, the material constants are determined using a least-square method to minimize the relative error in stress. Given N stress-strain data pairs, the relative error E is

$$E = \sum_{i=1}^{N} \left(1 - \frac{\sigma_i^{th}}{\sigma_i^{test}} \right)^2 \tag{5.11}$$

where σ_i^{test} is a stress value from test data and σ_i^{th} is the theoretical value derived from one of the strain energy functions.

5.1.4 Stability check

In Abaqus, a stability check is done for each material using the Drucker stability condition for three different deformation modes, uniaxial, equibiaxial and planar (pure shear) mode. The condition requires the inequality

$$\mathbf{d}\boldsymbol{\sigma}^T \mathbf{d}\boldsymbol{\varepsilon} > 0 \tag{5.12}$$

to be satisfied, where $\mathbf{d}\boldsymbol{\varepsilon}$ is a infinitesimal change of logarithmic strain and $\mathbf{d}\boldsymbol{\sigma}$ is the corresponding change of Cauchy stress. Using $\mathbf{d}\boldsymbol{\sigma} = \mathbf{D}\,\mathbf{d}\boldsymbol{\varepsilon}$, the condition yields in

$$\mathbf{d}\boldsymbol{\varepsilon}^T \mathbf{D}\,\mathbf{d}\boldsymbol{\varepsilon} > 0 \tag{5.13}$$

which requires the tangential stiffness matrix $\mathbf{D}$ to be positive definite.

5.2 Target curve

The target curve used in the fitting procedure is the static true stress-strain curve for PC/ABS, calibrated in [3] which is a prior thesis work at Sony Ericsson, c.f. Figure 5.1.

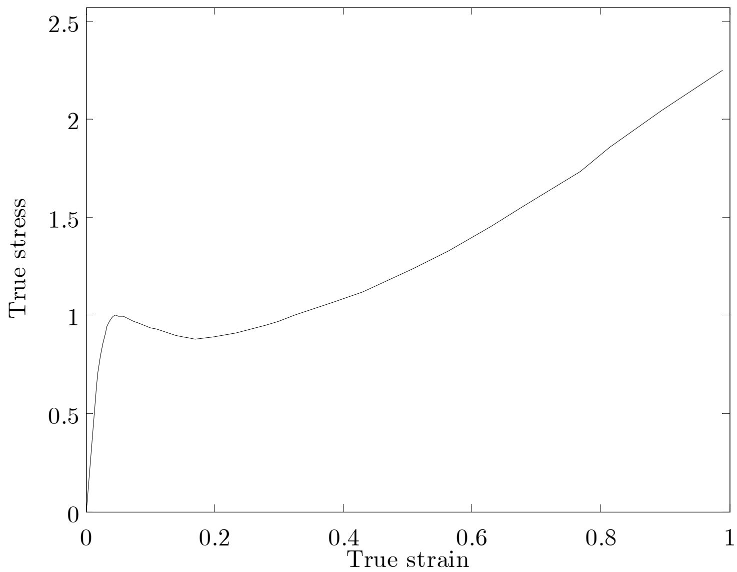

Figure 5.1: True stress-strain curve for static loading of PC/ABS [3]

By inserting data from only the first half of the curve, the fit will be better up to 50 % strain and totally useless above that strain level. The fitting procedure was therefore performed for up to four different strain levels, 100 %, 50 %, 30 % and 20 %.

5.3 Results

The fitted curves for the different strain levels are shown in Figure 5.2. Lower order functions, i.e. Neo-Hooke and Mooney-Rivlin are not capable of capturing the polymeric behavior. It can also be seen that Mooney-Rivlin, after the stress peak, goes towards a negative infinity.

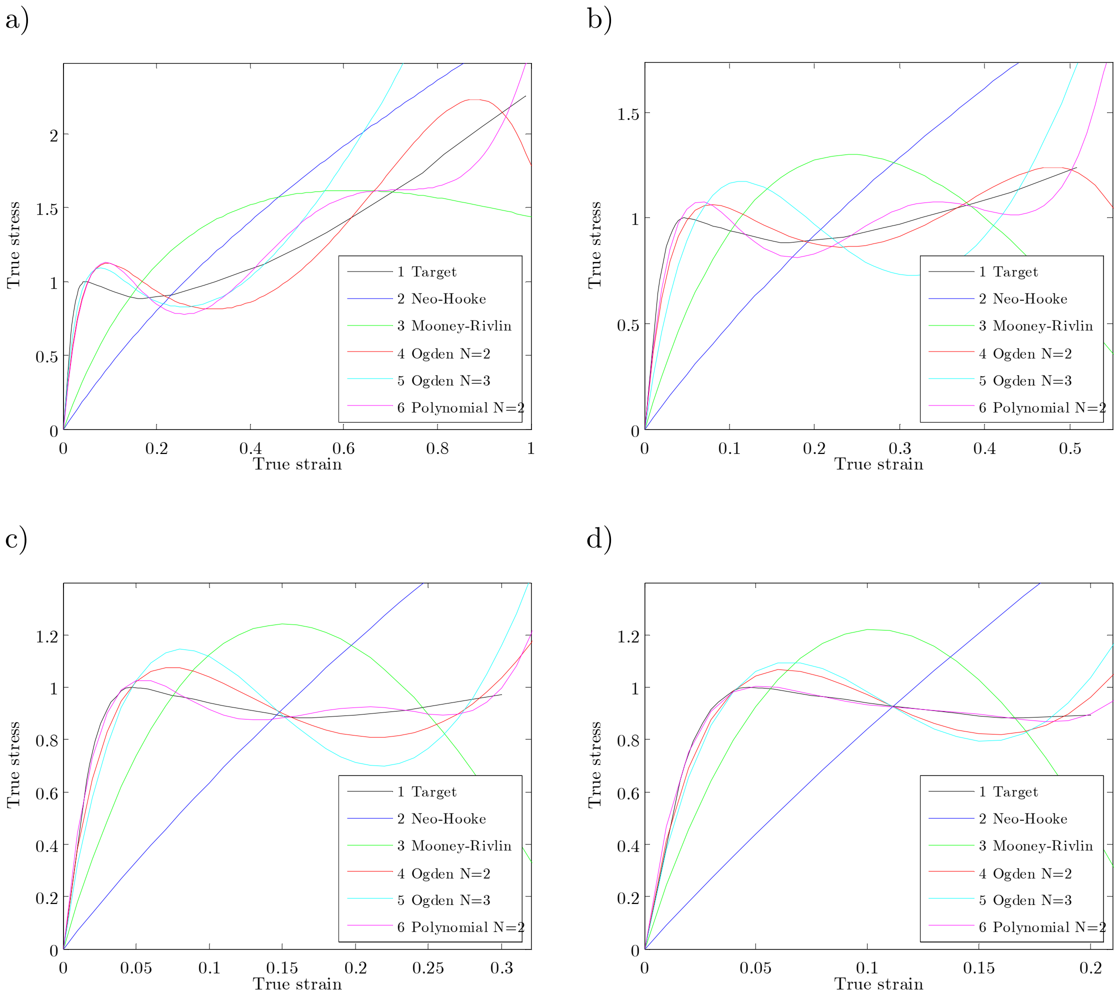

Figure 5.2: Fitted curves for a) 100 % b) 50 % c) 30 % d) 20 % strain

5.4 Discussion

As seen in Figure 5.2, the lower order functions are rather useless for this application. The function in question needs to be able to capture the initial hardening, the post-yield softening and the large strain hardening. It is a great advantage to know in advance what strain levels to expect in the analysis. Then one can choose a function with a better fit in the expected strain level region. However, the strain levels in the analysis must be smaller than range of the fitted function. Strain levels above that would lead to an unreasonable stiff material if the polynomial goes towards a positive infinity and a collapse of the model otherwise.
The result of the stability check was that each model was stable as long as the curve gradient was positive, i.e. the model became unstable when the softening started. However, this is only a problem when simulating unstable geometries such as tensile testing specimens with an implicit analysis. In explicit analyses, no equilibrium is calculated and hence, the unstable material is not a problem.

Based on this discussion, the function chosen was the general polynomial of the order of two, fitted for up to 50 % strains.

Chapter 6

A one-dimensional model

A one-dimensional model was implemented in Matlab in order to calibrate the constitutive models to experimental data. The constitutive equations were reduced to one dimension and further differentiated to time-rate form. An ODE (Ordinary Differential Equation) solver was used to integrate the constitutive equations. The constitutive model is illustrated in Figure 6.1. [27]

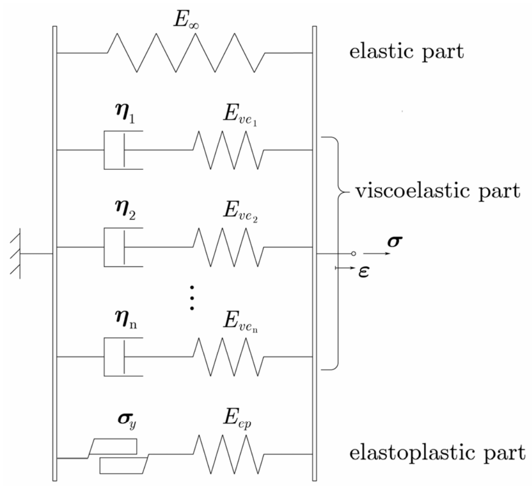

Figure 6.1: Constitutive model

6.1 Theory

6.1.1 Hyperelasticity

In the case of uniaxial loading, the stretch is calculated as

$$\lambda = \frac{L+\delta}{L} = 1+\varepsilon \tag{6.1}$$

where L is the original length of the specimen and δ its elongation. For simplicity, incompressibility is assumed and the condition $\lambda_1\lambda_2\lambda_3 = 1$ leads to

$$\begin{cases} \lambda_1 = \lambda_U \\ \lambda_2 = \lambda_3 = \dfrac{1}{\sqrt{\lambda_U}} \end{cases} \tag{6.2}$$

The first two strain invariants can then be obtained by inserting (6.2) into the general expressions for the strain invariants as

$$\begin{cases} I_1 = \dfrac{2}{\lambda} + \lambda^2 \\ I_2 = \dfrac{1}{\lambda^2} + 2\lambda \end{cases} \tag{6.3}$$

The nominal stress-strain relationship for an arbitrary stored strain energy function $W(I_1, I_2)$ can now based on (3.17) and (3.23) be derived as

$$\sigma = \frac{\partial W}{\partial \lambda_U} = \frac{\partial W}{\partial I_1}\frac{\partial I_1}{\partial \lambda_U} + \frac{\partial W}{\partial I_2}\frac{\partial I_2}{\partial \lambda_U} \tag{6.4}$$

6.1.2 Viscoelasticity

The stress response of a generalized Maxwell model with relaxation modulus as (3.30) can be expressed as

$$\sigma(t) = E_0\varepsilon(t) - \sum_{i=1}^{N} E_i\alpha_i \tag{6.5}$$

where the initial modulus and the relaxation times are defined as

$$\left.\begin{aligned} E_0 &= E_\infty + \sum_{i=1}^{N} E_i \\ \tau_i &= \eta_i / E_i \ , \quad i = 1, \ldots, N \end{aligned}\right\} \tag{6.6}$$

The internal variables α_i are governed by evolution as

$$\left.\begin{aligned}\dot{\alpha}_i + \frac{\alpha_i}{\tau_i} = \frac{\varepsilon}{\tau_i} \\ \lim_{t\to-\infty} \alpha_i(t) = 0\end{aligned}\right\} \tag{6.7}$$

This internal variable is replaced by a stress variable such as

$$q_i = E_i \alpha_i \tag{6.8}$$

A non-dimensional relative moduli $\gamma_i = E_i / E_0$ is introduced with the restriction

$$\gamma_\infty + \sum_{i=1}^{N} \gamma_i = 1 \tag{6.9}$$

where $\gamma_\infty = E_\infty / E_0$. By using a stored strain energy function $W(I_1, I_2)$ the time-dependent elastic stress-strain relationship takes the form

$$\left.\begin{aligned}\sigma &= \frac{\partial}{\partial \varepsilon} W(\varepsilon) - \sum_{i=1}^{N} q_i \\ \dot{q}_i + \frac{1}{\tau_i} q_i &= \frac{\gamma_i}{\tau_i} \frac{\partial}{\partial \varepsilon} W(\varepsilon) \\ \lim_{t\to-\infty} q_i(t) &= 0\end{aligned}\right\} \tag{6.10}$$

Using an arbitrary stored strain energy function $W(I_1, I_2)$ makes the model valid for nonlinear elastic response.

6.1.3 Plasticity

The structure of classical plasticity is illustrated by a frictional device shown in Figure 6.2. It consists of an elastic spring with elastic constant *E*, and a Coulomb friction element with constant $\sigma_y > 0$.

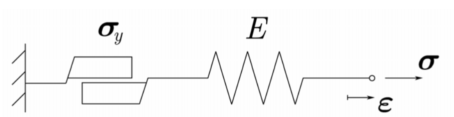

Figure 6.2: Friction element

The stress in the spring is given by the elastic modulus and gives the elastic relationship

$$\sigma = E\varepsilon^{e} = E(\varepsilon - \varepsilon^{p}) \tag{6.11}$$

Yield criteria

It has to be determined whether the current stress level is inside the elastic limit or not. For that reason the yield condition (3.35) is introduced. For perfect plasticity it is defined as

$$f(\sigma) = |\sigma| - \sigma_{y} \leq 0 \tag{6.12}$$

Evolution laws

For perfect plasticity in one dimension, the flow rule (3.45) is reduced to

$$\dot{\varepsilon}^{p} = \dot{\lambda}\frac{\partial f}{\partial \boldsymbol{\sigma}} = \dot{\lambda}\ \mathrm{sign}(\sigma) \tag{6.13}$$

The consistency relation $\dot{f} = 0$ yields

$$\begin{aligned} \dot{f} &= \frac{\partial f}{\partial \sigma} E(\dot{\varepsilon} - \dot{\varepsilon}^{p}) \\ &= \frac{\partial f}{\partial \sigma} E\dot{\varepsilon} - \dot{\lambda}\frac{\partial f}{\partial \sigma} E\,\mathrm{sign}(\sigma) \end{aligned} \tag{6.14}$$

Since $\partial f / \partial \sigma = \mathrm{sign}(\sigma)$ and $(\mathrm{sign}(\sigma))^2 = 1$, (6.14) leads to

$$\dot{\varepsilon}^{p} = \begin{cases} \dot{\varepsilon} & \textit{for} \quad f(\sigma) = \dot{f}(\sigma) = 0 \\ 0 & \textit{for} \quad f(\sigma) < 0 \end{cases} \tag{6.15}$$

6.2 Implementation

The constitutive equations are rewritten to time-rate form in order to be integrated in an ODE solver. Taking the time derivative of the function (6.10.a) yields in

$$\dot{\sigma}^{ve} = \frac{\partial^2}{\partial \varepsilon^2} W(\varepsilon)\dot{\varepsilon} - \sum_{i=1}^{N} \dot{q}_i \tag{6.16}$$

where $\dot{q}_i$ can be solved from (6.10.b). $W(\varepsilon)$ is an arbitrary stored strain energy function leading to

$$\dot{\sigma}^{ve} = \frac{\partial^2 W}{\partial \lambda_U^2} \dot{\varepsilon} - \sum_{i=1}^{N} \left(\frac{\gamma_i}{\tau_i} \frac{\partial W}{\partial \lambda_U} - \frac{1}{\tau_i} q_i \right) \tag{6.17}$$

The elasto-plastic response is given by the following algorithm.

Box 6.1: Check for elasto-plastic response

1. Initiziation:

$$\dot{\varepsilon}$$

2. Calculate trial plastic multiplier:

$$\dot{\lambda} = \mathrm{sign}(\sigma)\,\dot{\varepsilon}$$

3. Calculate yield function:

$$f = |\sigma| - \sigma_y$$

4. Check response

   if $f \geq 0$ and $\dot{\lambda} > 0$: plastic response

$$\dot{\sigma} = 0$$
$$\dot{\varepsilon}^p = \dot{\varepsilon}$$

   else: elastic response

$$\dot{\sigma} = E\dot{\varepsilon}$$
$$\dot{\varepsilon}^p = 0$$

5. Update variables:

$$\dot{\sigma}^{ep} = \dot{\sigma}$$
$$\dot{\varepsilon}^p$$

The total stress response is then given by the sum of the viscoelastic and the elasto-plastic stresses as

$$\dot{\sigma} = \dot{\sigma}^{ve} + \dot{\sigma}^{ep} \tag{6.18}$$

In order to calculate the reaction force, for calibration to test data, the compressibility had to be accounted for and hence, the force was calculated as

$$F = A\,\sigma \tag{6.19}$$

where

$$A = \frac{A_0}{1 + 2\nu\varepsilon} \tag{6.20}$$

6.3 Parameter identification

The parameters of the constitutive model have been fitted to experimental data for PC/ABS. Parameters to be fitted are presented in Table 6.1.

Table 6.1: Parameters to be fitted

E_∞	Hyperelastic part
γ_1	Viscoelastic part
γ_2	
γ_3	
τ_1	
τ_2	
τ_3	
E_{ep}	Elasto-plastic part
σ_y	

The parameter E_∞ is a hyperelastic multiplier which scales the constants in the hyperelastic polynomial equally, c.f. Figure 6.3. The polynomial with fitted constants is chosen from chapter 5 and is, in this fitting procedure, the general polynomial (N=2) fitted for 50 % strain.

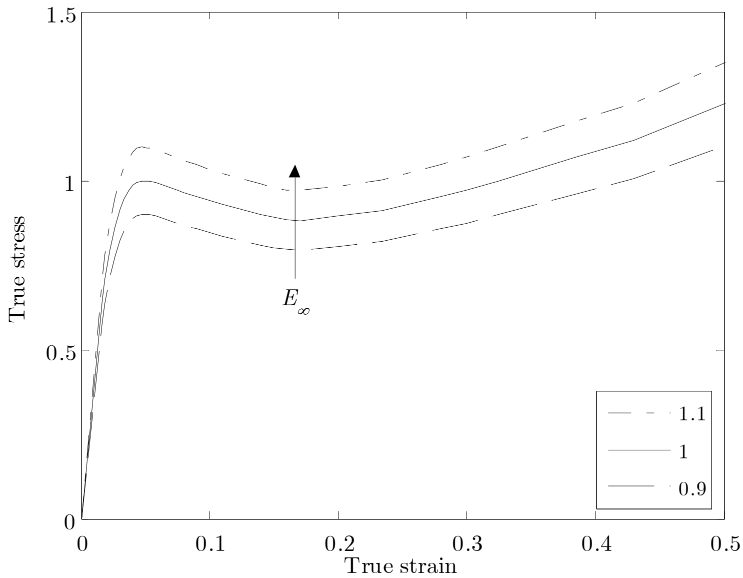

Figure 6.3: Effect of hyperelastic multiplier

The fitting procedure was a trial and error method and three different sets of parameters were fitted. One set for static analysis without any viscoelastic effects, one set for low strain rates and one set for high strain rates as in e.g. drop test simulations. The static curve was calibrated to a rate of displacement of 0.5 mm/min. The low strain rates set was calibrated to quasi-static tests (10 mm/min) up to 30 mm/s for simulations under a second. The set of parameters for high strain rates is for faster analyses up to corresponding 20 % strain in one millisecond (23000 mm/min).

All calibrations to test data were made to the load-displacement curve and the model could therefore only be fitted up to the point of necking. The only true stress-strain curve for PC/ABS available was the static loading curve.

Figure 6.4 shows three different areas of the curve where good fit is of extra importance. Area one is crucial for an overall true flexibility within the structure. Area two governs the rate dependency and the plastic flow and the third area determines the remaining damage after unloading and is of main interest in this thesis. The crosses indicate the location after one hour of recovery and hence, should be the target for a much better prediction of the remaining damage then the instant after unloading.

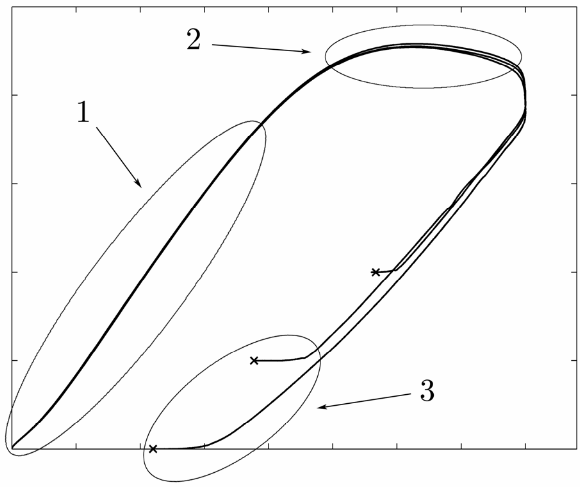

Figure 6.4: Areas of interest in the fitting procedure

A drawback in the Matlab model compared to Abaqus is the limitation of the elasto-plastic curve. The plasticity in the one-dimensional model is ideal plasticity whereas in Abaqus, an arbitrary hardening/softening plastic curve can be used for a better fit. The idea of the fitting procedure is to get a rough fit with the Matlab model and modify it with the elasto-plastic curve, c.f. Figure 6.5.

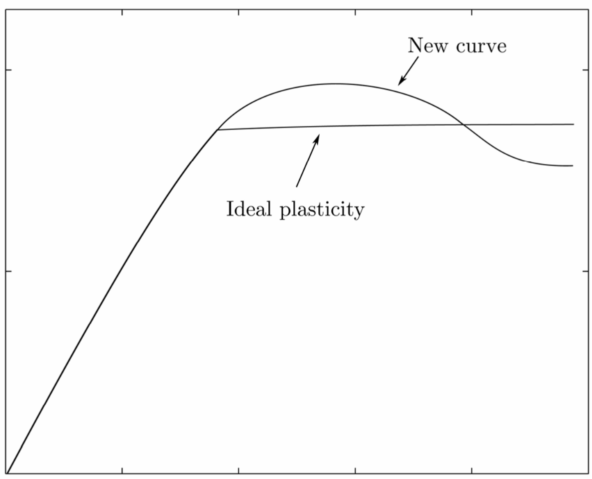

Figure 6.5: Trimming the elasto-plastic curve

6.4 Results

Figure 6.6 shows the material model with fitted parameters compared to experimental data in static loading. In Figure 6.7, the model is compared to the static loading true stress-strain curve for PC/ABS at higher strains. Figure 6.8 shows a comparison of the unloading between the new model and the old elasto-plastic model which unloads linearly with Young's modulus.

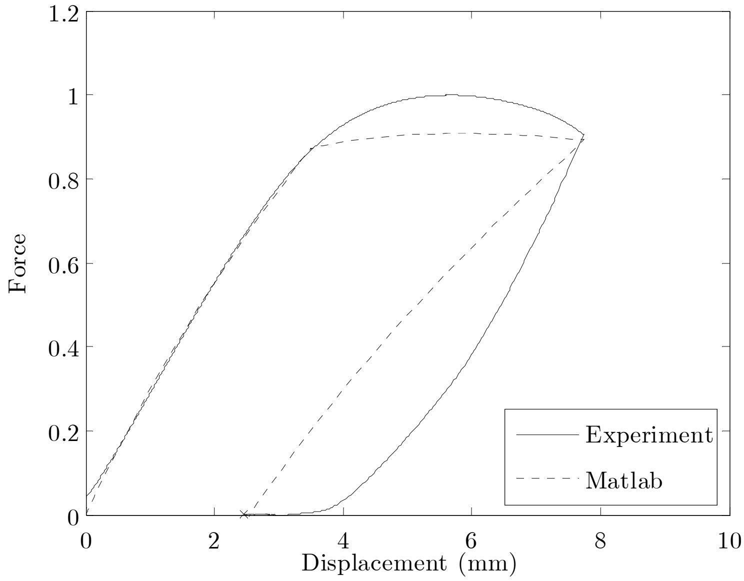

Figure 6.6: Fitted model compared to experimental data for static loading and unloading with 1 kN/s. The cross indicates the location after one hour's recovery.

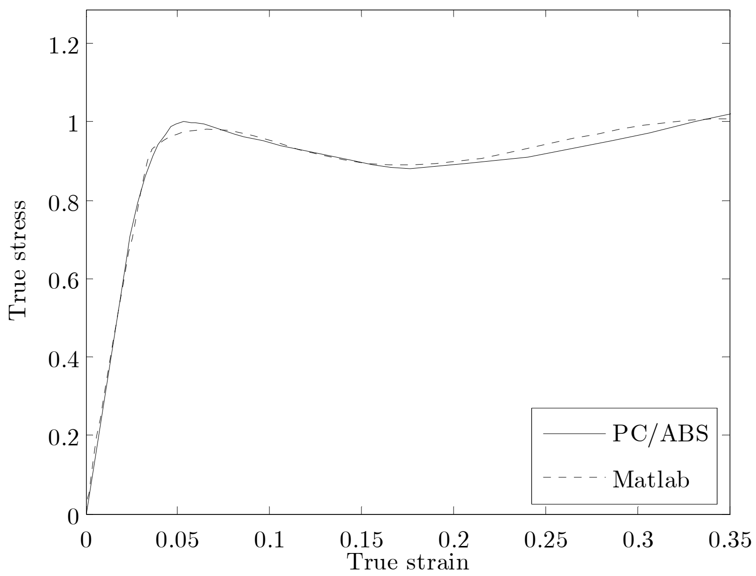

Figure 6.7: Matlab model compared to the true stress-strain curve for PC/ABS in static loading

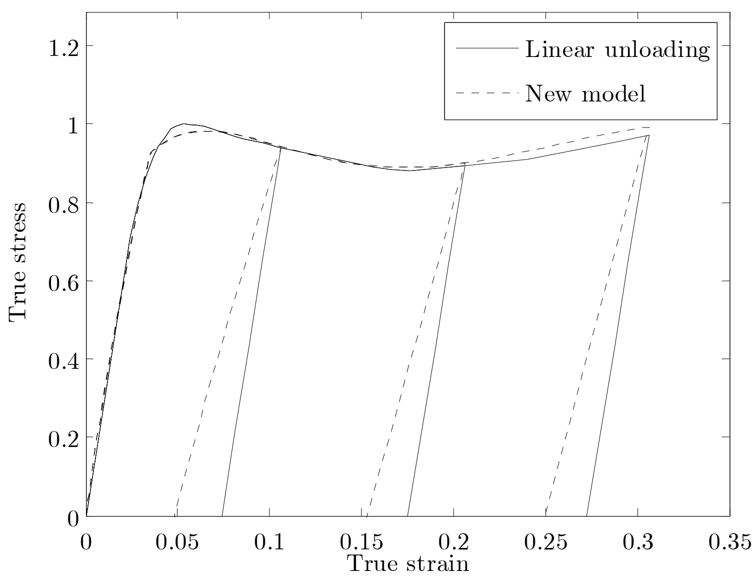

Figure 6.8: New model compared to an elasto-plastic model with linear unloading

Figure 6.9 shows the fitting curves for low strain rates analysis for different loading rates, unloading with 1 kN/s and one hour's recovery.

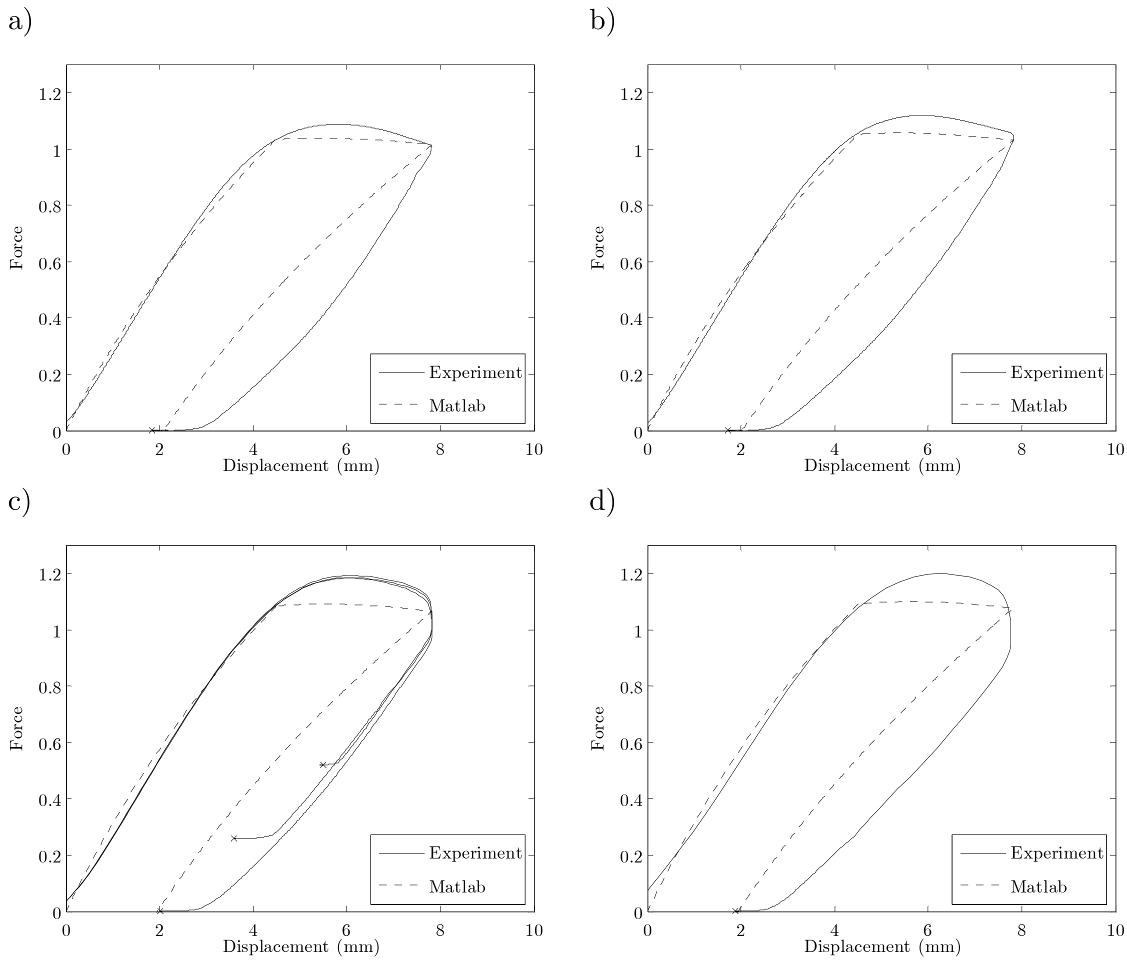

Figure 6.9: Fitted model for a) 10 mm/min b) 50 mm/min c) 10 mm/s d) 30 mm/s compared to experimental data. The crosses indicates the position after 1 hours recovery

Figure 6.10 shows the material model compared to experimental data for high strain rates. Curve a) is from an experiment and b)-d) are logarithmic extrapolated from curve a due to limitations in the testing equipment.

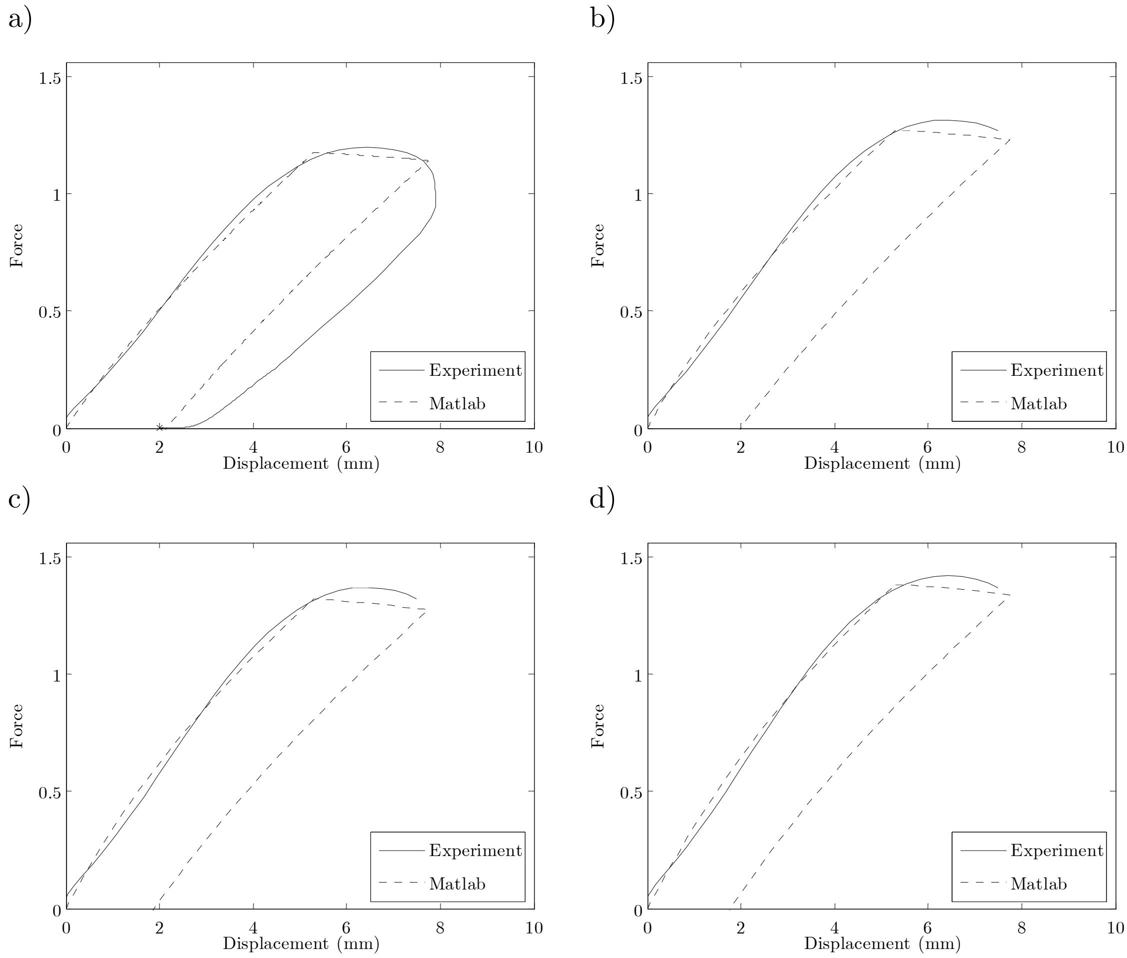

Figure 6.10: Fitted curves for a) 30 mm/s b) 1150 mm/s c) 5750 mm/s d) 23000 mm/s compared to experimental and extrapolated data.

Chapter 7

Abaqus verification

Three-dimensional simulations have been performed in Abaqus in order to verify the material model to experimental data. Due to convergence problems with the unstable hyperelastic model, most simulations were made with Abaqus/Explicit. Three different geometries have been simulated for different purposes.

- One unit element – Modify the constitutive model from the Matlab simulations
- Test specimen – Verify the model to experimental data (uniaxial tensile tests)
- Bending test – Verify the model in a tension/compression stress state

The element type used in Abaqus/Explicit was C3D8R, which is a first order eight-node brick element with reduced integration.

7.1 Theory

7.1.1 Explicit dynamic solver method

The method is based on central difference formulas for the velocity and the acceleration. In Abaqus the explicit dynamic procedure is based upon the implementation of an explicit integration rule and the use of diagonal or lumped element mass matrices. The equations of motion are described with the explicit central difference integration rule [11]

$$\dot{\mathbf{u}}^{(i+\frac{1}{2})} = \dot{\mathbf{u}}^{(i-\frac{1}{2})} + \frac{\triangle t^{(i+\frac{1}{2})} + \triangle t^{(i)}}{2} \ddot{\mathbf{u}}^{(i)} \tag{7.1}$$

and

$$\mathbf{u}^{(i+1)} = \mathbf{u}^{(i)} + \triangle t^{(i+1)} \dot{\mathbf{u}}^{(i+\frac{1}{2})} \tag{7.2}$$

where $\triangle t$ is defined as

$$\triangle t^{i} = t^{i+\frac{1}{2}} - t^{i-\frac{1}{2}} \tag{7.3}$$

$\dot{\mathbf{u}}$ and $\ddot{\mathbf{u}}$ is velocity and acceleration and the superscript i refers to the increment number. The velocities are defined at the midpoint of the time intervals, so called half-steps or midpoint steps. Using known values of $\dot{\mathbf{u}}^{(i-\frac{1}{2})}$ and $\ddot{\mathbf{u}}^{(i)}$ from the previous increment the kinematic state can be obtained explicitly.

To make the explicit procedure computationally efficient, diagonal element mass matrices are used since its inversion used in the beginning of the increment is triaxial. The procedure requires no iterations and no tangent stiffness matrix.

$$\ddot{\mathbf{u}}^{(i)} = \mathbf{M}^{-1}(\mathbf{F}^{(i)} - \mathbf{I}^{(i)}) \tag{7.4}$$

where $\mathbf{M}$ is the diagonal lumped mass matrix, $\mathbf{F}$ is the applied load vector, and $\mathbf{I}$ is the internal force vector, which is dependent on the current stress state.

When the acceleration is calculated for increment i in (7.4) all information needed is given so that the displacement for $i+1$ using equation (7.1) can be calculated.

The explicit method is only conditionally stabile, which means that there are restrictions on the size of the time step. The length of the critical time step is dependent on the elastic behavior, the bulk modulus and least element size among others. [17] [14]

7.1.2 Material

The constitutive model used in the simulations was the combined viscoelastic- elasto-plastic model implemented with the overlay method.

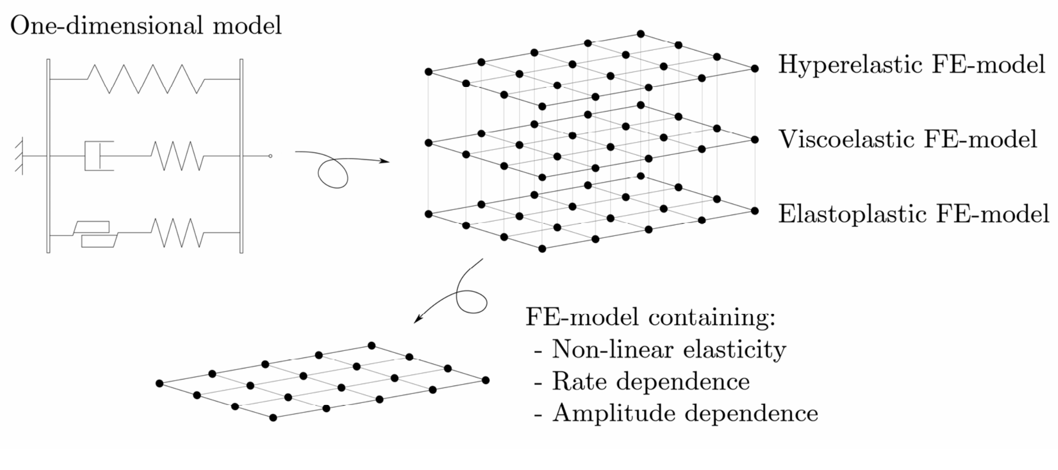

Figure 7.1: Principle of the overlay method

In order to implement this method, the keyword *ELCOPY was used to create a double mesh, i.e. two identical solid sections with different materials. One material is the hyperelastic material with a viscoelastic part and the other material is an isotropic elasto-plastic material.

7.1.3 Mass scaling

When simulating time-dependent models, a step time of the magnitude of seconds is required. By using the maximum stabile time increment for a plastic material with a reasonably fine mesh, the simulation would take several weeks for a tensile test and because of the large number of increments, the round-off errors would be severe. In order to minimize the simulation time for long test times a mass scaling method was used. The factor that determines the simulation time is the maximum stabile time increment which can be estimated as [11]

$$\Delta t_{stable} \leq \min\left(L_e\sqrt{\frac{\rho}{\hat{\lambda}+2\hat{\mu}}}\right) \tag{7.5}$$

where L_c is a characteristic length for the element and ρ is the density of the material. The minimum is taken over all elements in the mesh and $\hat{\lambda}$ and $\hat{\mu}$ are the effective Lamé's constants, in an isotropic elastic material defined as

$$\hat{\lambda} = \lambda_0 = \frac{E\nu}{(1+\nu)(1-2\nu)} \tag{7.6}$$

and

$$\hat{\mu} = \mu_0 = \frac{E}{2(1+\nu)} \tag{7.7}$$

The method is used by setting the desirable time increment Δt and the ratio between the chosen and the stabile time increment determines the mass scaling as

$$\frac{\rho_{scaled}}{\rho} = \left(\frac{\Delta t}{\Delta t_{stable}}\right)^2 \tag{7.8}$$

A higher density would lead to erroneous reaction forces due to dynamic effects in faster analyses. The method of mass scaling was therefore only used in the analyses with long simulation times. The time increment used in the long analyses was about 10 times the stable increment and hence, the mass scaling was about 10^2 times or 10^4 %. As long as the force curve is smooth, the mass scaling should not affect the result.

7.2 Unit element

The purpose for the simulation of a unit element was to adjust the loading curve for a better fit to the static true stress strain curve by modifying the elasto-plastic part of the model. Of the three sets of parameters fitted in chapter 6 only the static set could be compared to true stress-strain data. For that reason, only the static set of parameters was used in the simulation of a unit element. The elasto-plastic part of the rate dependent parameter sets were then assumed to have the same shape as the static curve and could therefore be calculated from the static curve.

7.2.1 Modelling

The unit element was modelled as a cube with unit length one. Zero displacement boundary conditions were applied at one side and a given displacement at the opposite side, cf. Figure 7.2. The analysis was performed in Abaqus/Standard, i.e. in an implicit solver, with a static load step.

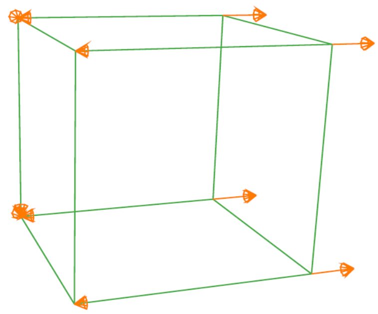

Figure 7.2: Boundary conditions

7.2.2 Results

The result of the modification of the elasto-plastic curve is show in Figure 7.3. It is the same model as in Figure 6.7 but with a modified elasto-plastic curve instead of the ideal plastic, both combined with non rate dependent hyperelasticity. The plastic curve in the rate dependent models were assumed to have the same shape so the static curve was only moved to new yield stresses.

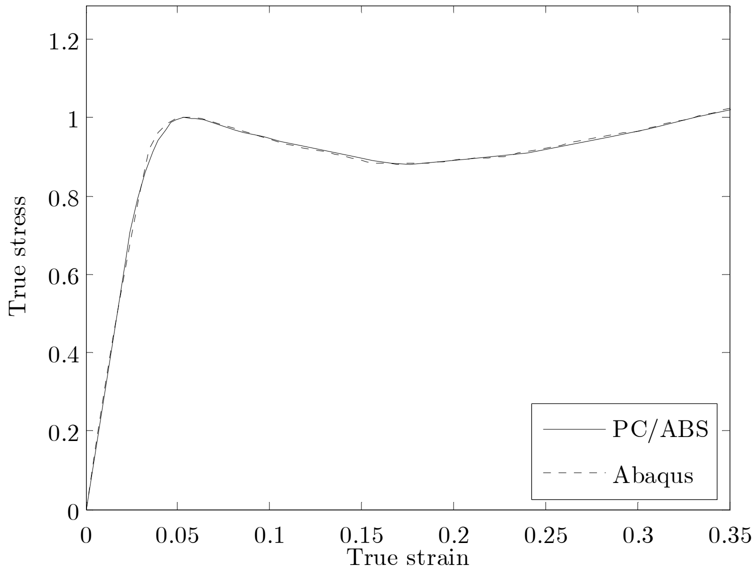

Figure 7.3: Adjusted model compared to the true stress-strain curve for PC/ABS in static loading.

7.3 Test specimen

The tensile tests in chapter 5 have been simulated in Abaqus/Explicit in order to verify the constitutive model to experimental data. A fully three-dimensional simulation is required to capture the effect of necking and for obtaining the same force-displacement curve as in the experiments.

7.3.1 Modelling

The test specimen modelled was the ISO-standard bar with dimensions as in Figure 4.1. In order to minimize the simulation time three symmetry planes was used so that only one eighth of the specimen had to been modelled. The model was meshed with brick elements with a refinement in the middle of the bar. An imperfection was made at the middle of the bar to control the initiation of necking. The width of the cross section was decreased over one element with 1 %, cf. Figure 7.4.

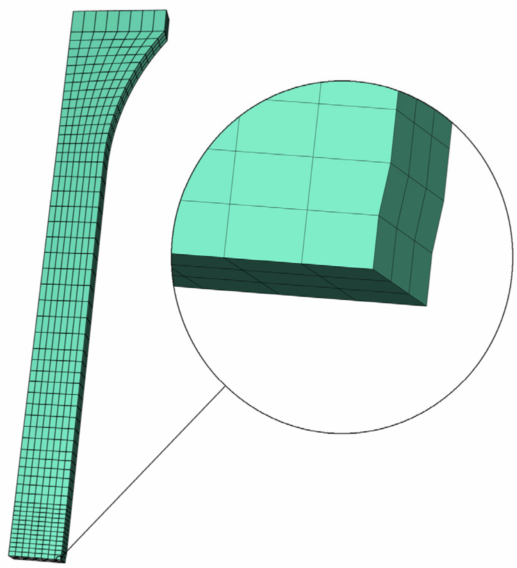

Figure 7.4: Finite element model of a test specimen

To be able to obtain the total force in the bar, a MPC (Multi Point Constraint) was used, cf. Figure 7.5. It can be interpreted as if the nodes on the top surface are connected to an external node with stiff elements. Boundary conditions were then applied on the node instead of the surface and hence, the total reaction force could be extracted from the simulation.

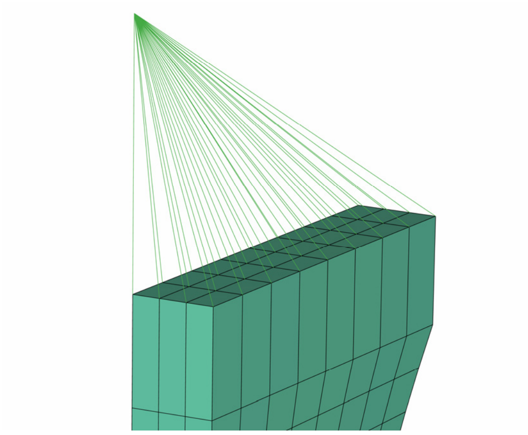

Figure 7.5: Multi Point Constraint

Zero displacement boundary conditions were applied on the three symmetry surfaces. Displacement control was used and applied as a boundary condition in shape of a linear ramp with constant velocity. The displacement rate was controlled by the step time.

7.3.2 Results

Figure 7.6 shows a specimen after loading to 8 mm at 1150 mm/s and an initiation of necking in the middle of the specimen is clearly visible. The contours in the plot are max principle logarithmic strain.

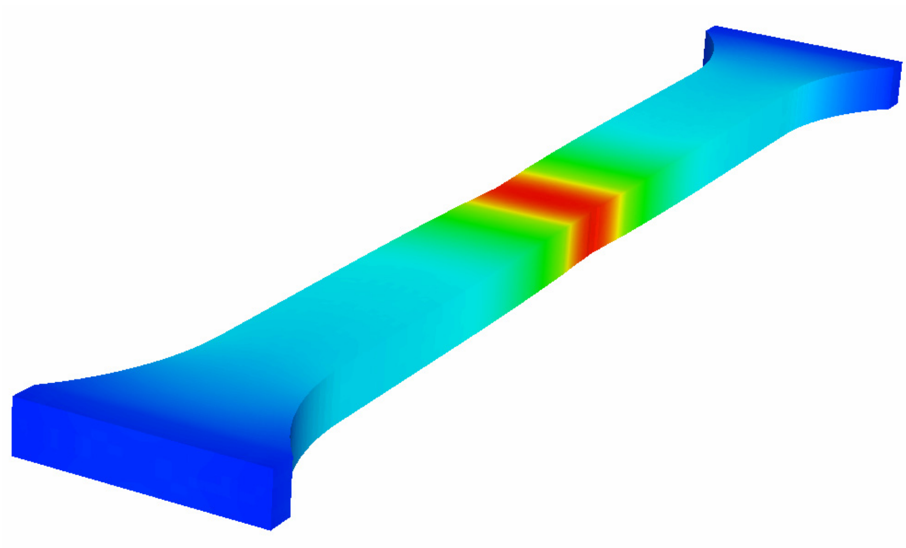

Figure 7.6: Specimen after loading to 8 mm at 1150 mm/s

Figure 7.7 shows an Abaqus simulation of loading and unloading to 8 mm compared to the experiment at 0.5 mm/min. The material model used was the static, i.e. rate-independent model.

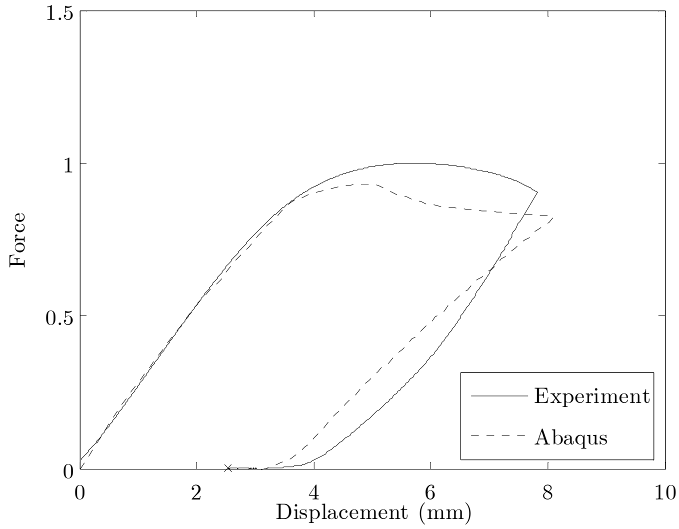

Figure 7.7: Static model compared to experiment to 8 mm at 0.5 mm/min

Figure 7.8 shows simulations compared to experiments with a strain rate of 10 mm/s during loading and unloading with one hour's recovery. In a), different unloading levels have been tested and different strain levels (8, 10 and 15 mm) have been tested and simulated in b). The material model used in the simulations was the low strain rate model.

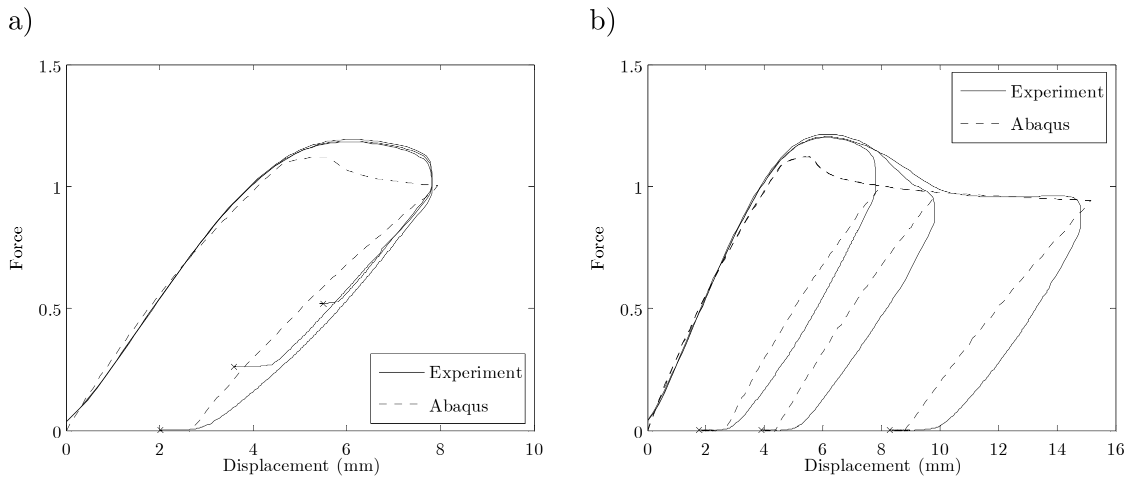

Figure 7.8: Simulations compared with experiments to a) 8 mm b) 8, 10 and 15 mm, at 10 mm/s

Figure 7.9 shows simulations of different high strain rate experiments. Curve a) is an experimental curve at 30 mm/s and b)-d) are logarithmic extrapolated from curve a). Only the experimental curve is represented with unloading.

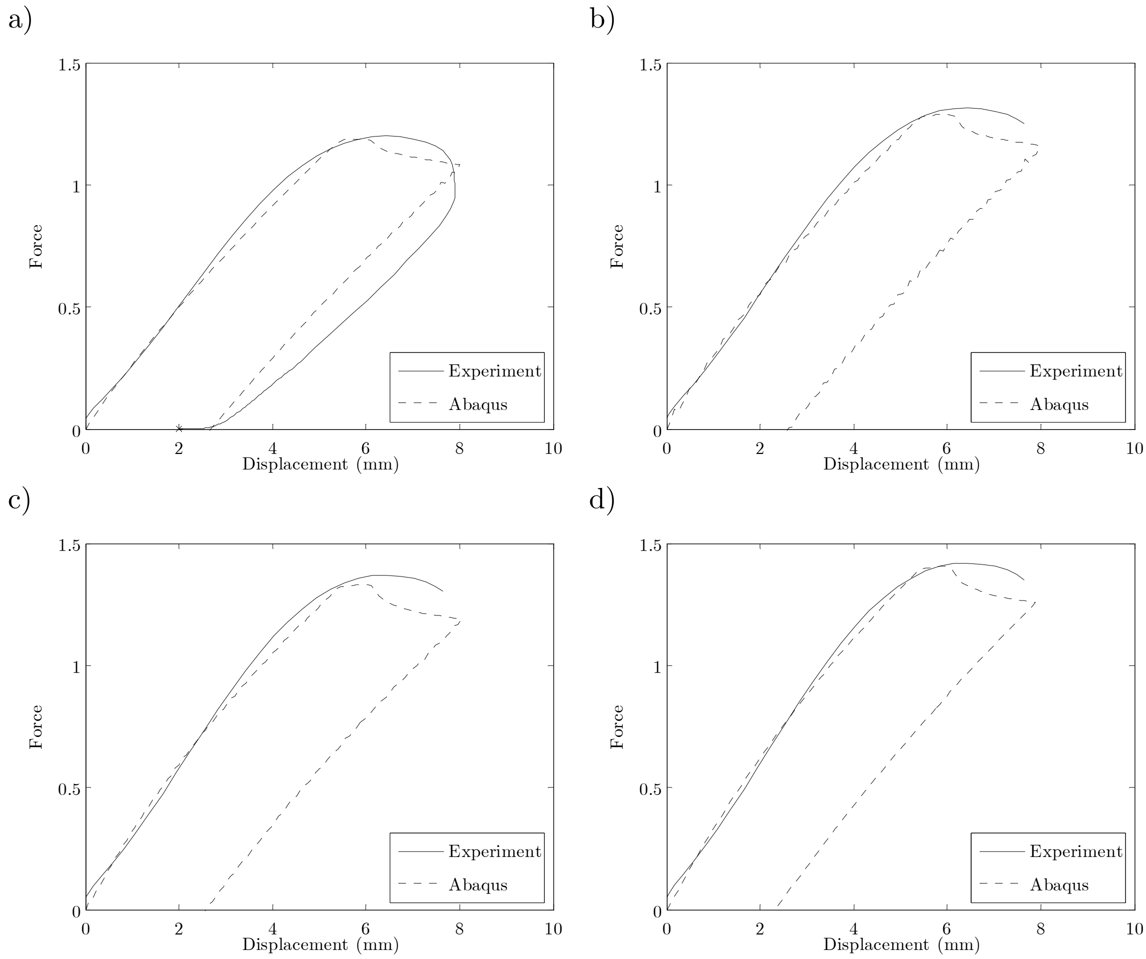

Figure 7.9: Simulations compared to experiments to 8 mm at a) 30 mm/s b) 1150 mm/s c) 5750 mm/s d) 23000 mm/s

7.4 Bending test

The bending test described in chapter 5 has been simulated in Abaqus/Explicit in order to verify the constitutive model in a tension/compression stress state. Bending is a common type of deformation in a mobile phone simulation and should therefore be a good measure of the models capabilities.

7.4.1 Modelling

The bending test setup was modelled with dimensions as in Figure 5.6. The test specimen was modelled as a beam with brick elements (C3D8R) with a refinement in the middle and courser mesh at the ends, c.f. Figure 7.10. The bearings and the probe were modelled with one layer of solid brick elements with the properties of steel, with nodes connected to a center node with stiff beams, c.f. Figure 7.11.

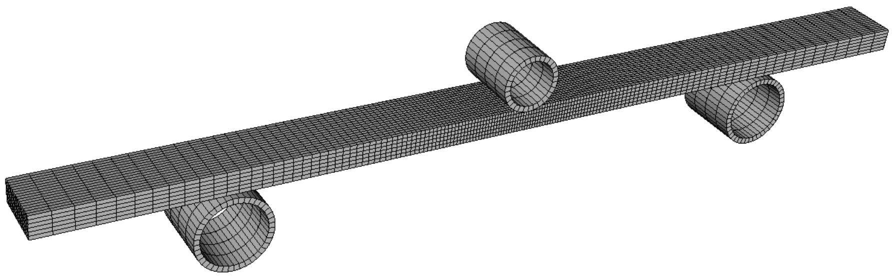

Figure 7.10: Model of bending test setup

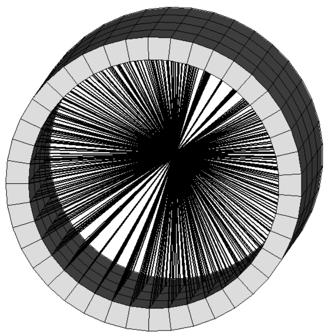

Figure 7.11: Model of probe

The bearings were locked in all degrees of freedom and the displacement was applied on the probe in shape of a smooth step. The contacts were modelled without friction with a general contact option.

Two different loading speeds were modelled to different displacements as the experimental bending test. The material models used was the static model for the slow tests and for the faster tests the parameters for the low strain rate model were used.

7.4.2 Results

Figure 7.12 shows the deformed specimen after loading to 40 mm. The contours show max principle logarithmic strain and it is visible that the strains are higher on the under side of the specimen, i.e. the tensile strains are higher than the compressive strains.

Figure 7.12: Deformed specimen in a bending test simulation to 40 mm

In Figure 7.13, Abaqus simulations are compared to experiments with a displacement rate of 4 mm/min with a strain rate corresponding to the static curve in the tensile tests. Figure 7.14 shows the model compared to experiments at 20 mm/s, simulated with the low strain rate model. The reaction force in the center node of the probe is plotted versus the vertical displacement.

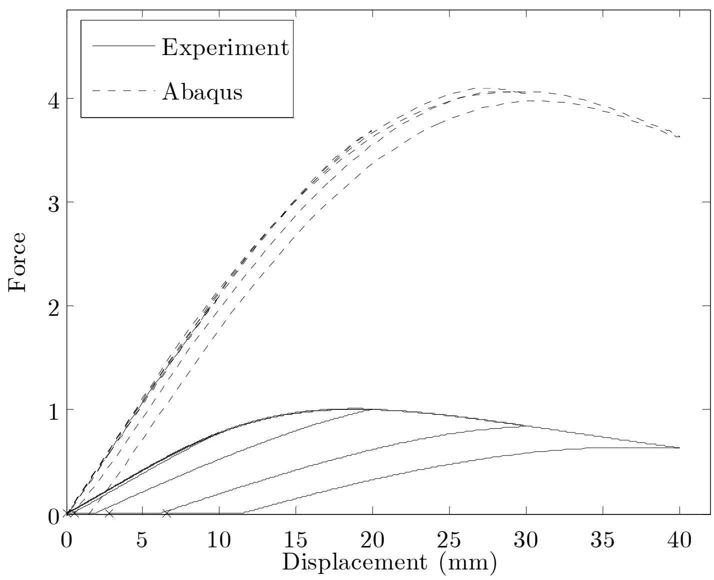

Figure 7.13: Bending test simulations compared to experiments at 4 mm/min

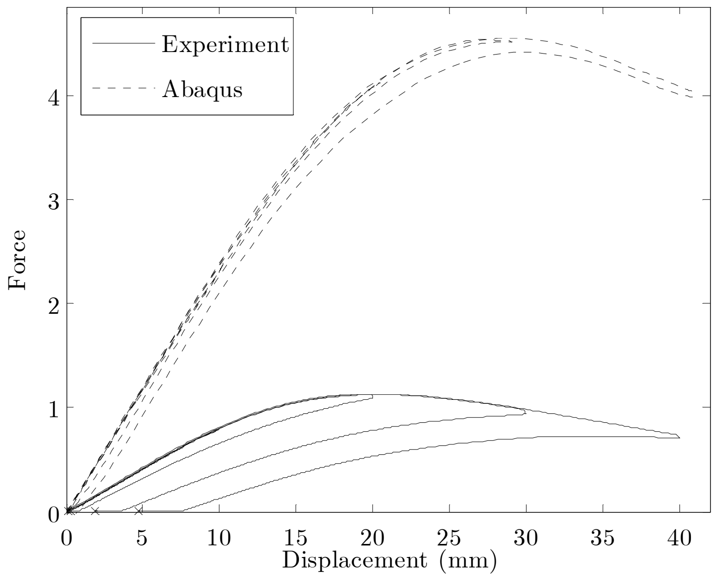

Figure 7.14: Bending test simulations compared to experiments at 20 mm/s

7.5 Discussion

After the modification of the elasto-plastic curve, the simulated true stress-strain curve showed good agreement with the target curve during uniaxial static loading. The calibrated parameters in Table 7.1 suggests that not only the elasticity is time-dependent, but also the plasticity.

Up to the point of neck initiation, the model shows good agreement with the experiments in the tensile tests. However, the model had difficulties in simulating the necking phenomenon. In real experiments, the initiation of necking is a continuous process where the polymer chains relocate whereas in the simulations, this process cannot be simulated and the neck forms too rapidly. Even the initiation of necking starts too early. In the experiments, no sign of a neck was visible after a displacement of 8 mm whereas Figure 7.6 clearly shows an initiation of a neck.

The fact that the force level is incorrect after loading completion makes the unloading false. The simulations show an overestimation of the remaining displacement after unloading because it starts on a lower force level. After formation of the neck, the model again shows good agreement with the simulation during loading.

In the simulations of the bending test, the model shows a far too stiff behavior. In contrary to the elasto-plastic model, the hyperelasticity has different properties in compression then in tension. The hyperelastic polynomial was fitted up to 50 % tensile strain which resulted in a poor fit in compression so for only small compressive strains, the fitted polynomial gets very stiff. This is particularly evident in the bending test where the upper side of the specimen is subjected to compressive strain and makes the specimen far to stiff. It also results in a more u-shaped form of the specimen after loading whereas in the experiments, the specimen was more v-shaped. Because of this, the strains on the upper and lower surfaces are less in the simulations and hence, the plastic strains are less which leads to an underestimation of the remaining damage after unloading.

To be able to use this model a new hyperelastic polynomial must be fitted to both tension and compression or alternatively, find a polynomial with the same properties in compression as in tension. Simulation of unstable geometries and necking is not trivial and not either a goal with this thesis so therefore, the bending test should be a more interesting measure of the capabilities of the material model.

Chapter 8

Concluding remarks

8.1 Summary

The Master's Thesis started out with an investigation of suitable material models for the thermoplastic PC/ABS. A desired model would be able to capture the mechanisms found in experimental testing like large strain elasticity, rate dependence, amplitude dependence, creep and damage. Such a model does not exist today. To complicate it even further the material appeared to be time dependent both in elasticity and in plasticity cf. Table 7.1. Restrictions made the selection limited to, in Abaqus, already existing models. The model chosen consists of an elasto-plastic model combined with a general Maxwell model based on hyperelasticity for the rate dependence. A hyperelastic strain energy function is a polynomial function of strain invariants. To calibrate the parameters a polynomial of higher order was needed since the function has to capture the initial hardening, the post-yield softening and the large strain hardening. The Abaqus function for fitting of hyperelastic constants to experimental data was used. The function chosen was a general polynomial of second order, fitted for up to 50 % tensile strains. Lower order functions, e.g. Neo-Hooke and Mooney-Rivlin are not capable of capturing the desired behavior.

A one-dimensional model was implemented in Matlab in order to calibrate the constitutive model to experimental data. It was difficult to fit the parameters to both static and higher strain rate tensile tests. Instead, three different sets of parameters were fitted. One set for static analysis without any viscoelastic effects, one set for low strain rate analyses and one set for high strain rates as in e.g. drop test simulations. The expected strain rates can most of the times be estimated before the analysis and the right set of parameters can be chosen.

Three-dimensional simulations where performed in Abaqus to verify the material model to experimental data, i.e. tensile and bending tests. Fully three-dimensional simulations were required in order to capture the necking phenomenon in tensile testing. The model showed to have difficulties with the necking instability and it both initiated and completed the formation of the neck too quickly. This also effected the unloading and the remaining deformation after unloading was therefore overestimated.

In the final verifications, the bending test simulations, the model showed a far too stiff behavior. The hyperelasticity has different properties in tension and compression and for even small compressive strains, the model gets too stiff.

Even though, the weaknesses in simulating necking and compression, the model showed good capabilities in capturing most of the mechanisms in the material.

8.2 Future work

The material model proved to be stiffer when simulating the specimen in bending comparing to experimental results. An investigation of polynomials considering material behavior in compression would therefore be necessary before using this model. To improve the model further, also the plasticity would need to be time-dependent. This could easily be implemented by introducing a power law for the plasticity.

Other tests of interest would be biaxial and shear tests to investigate how the material behaves in a multiaxial stress state. The shear properties are in many material model important input data.

As discussed in chapter 4, it is difficult to measure true stress-strain in a uniaxial tensile test. There are no simple existing methods today. Cameras taking snap shot pictures of the deformation of the cross-sectional area of the specimen are one method. A suggestion would be to develop such a method for Sony Ericsson's laboratory.

After a material model is selected, further improvements can be achieved in the fitting procedure where a least-square type of method could be used.

The model investigated in this thesis is a shortcut to describe a complex material behavior by combining, in Abaqus, already existing models. A desired model would be a single model with the ability to capture all the mechanisms in the material. Abaqus is currently working on a rate dependent $\mathbf{F}^e\mathbf{F}^p$-model. That is an elasto-plastic model based on hyperelasticity suitable for large deformations. At present, the model is implemented without rate dependency as a subroutine which can be purchased from Abaqus.

A more expensive alternative regarding resources would be to implement Anand's and Ames' model [18] as a user material subroutine in Abaqus. The model seems to capture many of the mechanisms in thermoplastics with satisfying results, at least in compression.

References

[1] Askeland D.R., (1996), *The Science and Engineering of Materials*, Thomson-Engineering

[2] Parsons E., Boyce M.C., Parks D.M. (2004), *An experimental investigation of the large-strain tensile behavior of neat and rubber-toughened polycarbonate*, Polymer 45, 2665–2684

[3] Persson H., Ådán K., (2004), *Modelling and experimental studies of PC/ABS at large deformations*, Master thesis, Division of Solid Mechanics, Lund University

[4] Utracki L.A., (1989), *Polymer Alloys and Blends*, Carl Hanser Verlag

[5] Balakrishnan S., Neelakantan N.R., Nabi Saheb D., Jyoti P. Jog (1998), *Rheological and morphological behavior of blends of polycarbonate with unmodified and maleic anhydride grafted ABS*, Polymer 39, 5765–5771

[6] Tjong S.C., Jiang Wei (1999), *Mechanical Performance of Ternary In Situ Polycarbonate/Poly(acrylonitrile-butadiene-styrene)/Liquid Crystalline Polymer Composites*, Journal of Applied Polymer Science 74, 2274–2282

[7] Din K.J., Hashemi S. (1997), *Influence of short-fibre reinforcement on the mechanical and fracture behavior of polycarbonate/Acylonitrile Butadiene Styrene polymer blend*, Journal of Material Science 32, 375-387

[8] Krenk S., (2005), *Non-Linear Modelling and Analysis of Structures and Solids*, Lecture notes, Division of Solid Mechanics, Lund University

[9] Belytschko T., Liu K.W, Moran B. (2000), *Nonlinear Finite Elements for Continua and Structures*, John Wiley & Sons Ltd.

[10] Ottosen N.S., Ristinmaa M., (2005), *The Mechanics of Constitutive Modelling*, Elsevier

[11] ABAQUS, Inc. (2006), *ABAQUS Reference Manuals*

[12] Ferry J.D., (1980), *Viscoelastic Properties of Polymers*, John Wiley & Sons Inc.

[13] Boyce M.C., Parks D.M., Argon A.S., (1988), *Large inelastic deformation of glassy polymers. Part 1: rate dependent constitutive model*, Mechanics of Materials 7, 15-33

[14] Arruda E.M., Boyce M.C., (1993), *Evolution of plastic anisotropy in amorphous polymers during finite straining*, International Journal of Plasticity 9, 697-720

[15] Wu P.D., Van der Giessen E., (1993), *On improved network models for rubber elasticity and their applications to orientation hardening of glassy polymers*, Journal of the Mechanics and Physics of Solids 41, 427-456

[16] Anand L., Gurtin M.E., (2003), *A theory of amorphous solids undergoing large deformations, with applications to polymeric glasses*, International Journal of Solids and Structures 40, 1465-1487

[17] Hasan O.A., Boyce M.C., (1995), *A constitutive model for the nonlinear viscoelastic viscoplastic bahavior of glassy polymers*, Polymer Engineering and Science 35, 331-344

[18] Anand L., Ames N.M., (2006), *On modelling the micro-identation response of an amorphous polymer*, International Journal of Plasticity 22, 1123-1170

[19] Simo J.C., (1987), *On a fully three-dimensional finite-strain viscoelastic damage model: formulation and computational aspects*, Computer Methods in Applied Mechanics and Engineering 60, 153-173

[20] Miehe C., Keck J., (2000), *Superimposed finite elastic-viscoelastic-plastoelastic stress response with damage in filled rubbery polymers. Experiments, modelling and algorithmic implementation*, Journal of the Mechanics and Physics of Solids 48, 323-365

[21] Lin R.C., Schomburg U., (2003), *A finite elastic-viscoelastic-elastoplastic material law with damage: theoretical and numerical aspects*, Computer Methods in Applied Mechanics and Engineering 192, 1591-1627

[22] Austrell, P.E., Olsson, A.K., (2003), *Modelling amplitude dependent dynamics of rubber by standard FE-codes*, Submitted to Journal of Engineering Mechanics, ASCE

[23] Haward R.N., Young R.J. (1997), *The Physics of Glassy Polymers*, Chapman & Hall

[24] Parsons E., Boyce M.C., Parks D.M., Weinberg M. (2005), *Three-dimensional large-strain tensile deformation of neat and calcium carbonate-filled high-density polyethylene*, Polymer 46, 2257–2265

[25] Inberg J.P.F., Gaymans R.J. (2002), *Polycarbonate and co-continuous polycarbonate/ABS blends: influence of specimen thickness*, Polymer 43, 3767-3777

[26] GE Plastics, (2006)

[27] Simo J.C., Hughes T.J.R., (1998), *Computational Inelasticity*, Springer-Verlag New York Inc.